Exploring Bessel beams, Airy beams, and Hydrogen-like linear bullets

Matthew S. Mills

The College of Optics & Photonics

University of Central Florida

Candidacy Examination

July 26th, 2012

Contents

List of Figures

Chapter 1

Introduction

1.1 Foreword

Sometimes certain well understood natural phenomena surprise us by acting in an unexpected manner. Not surprisingly, these anomalies attract the most interest which results in large amount of scientific effort. Three exciting examples of these phenomena are the Bessel beam [1], the Airy beam, [2], and the hydrogen-like bullets. These beams seemingly defy the long understood process of diffraction and dispersion, the spreading of light in space and time. Stranger yet, the Airy beam is a wavefront that curves in a parabolic fashion even in vacuum. Because of their novel properties, these beams may become valuable to applications ranging from detection of objects [3] to microlithography [4] to biological tissue sampling [5]. This candidacy report briefly summarizes some of the accumulated scientific knowledge concerning the Bessel beam and the Airy beam. Finally, the hydrogen-like bullets are put in context of other spatio-temporal bullets and then discussed in detail.

1.2 Derivation of the Helmholtz equation

The process of diffraction is a process related to the wave characteristic of light. It is derived from the Latin word diffringere which means “to break into pieces" [6]. In the words of Arnold Sommerfeld, diffraction consists of any deviation a

light ray takes from a rectilinear path that cannot be explained as reflection or refraction. In this process, the amplitude and phase of a wavefront is altered as it propagates because of lateral confinement [7]. Mathematically, one can begin with Maxwell's equations to describe the evolution dynamics of electromagnetic waves propagating in lossless vacuum.

$$\nabla \cdot \vec{E}(x,y,z,t) = 0 \tag{1.1a}$$

$$\nabla \cdot \vec{H}(x,y,z,t)\mu_0 = 0 \tag{1.1b}$$

$$\nabla \times \vec{E}(x,y,z,t) = -\mu_0 \frac{\partial \vec{H}(x,y,z,t)}{\partial t} \tag{1.1c}$$

$$\nabla \times \vec{H}(x,y,z,t) = -\epsilon_0 \frac{\partial \vec{E}(x,y,z,t)}{\partial t} \tag{1.1d}$$

Where $\vec{E}(x,y,z,t)$ is the electric field, $\vec{H}(x,y,z,t)$ is the auxillary magnetic field, μ_0 is the permeability of free space, and ϵ_0 is the permittivity of free space. By convention, the $\hat{z}$ direction is the propagation direction and the $\hat{x}$ and $\hat{y}$ are the coordinates transverse to the propagation. By using the relationship $\nabla \times \nabla \times \vec{E} = -\nabla^2 \vec{E} + \nabla(\nabla \cdot \vec{E})$ and combining (1.1a), (1.1c), and (1.1d), one arrives at the wave equation.

$$\nabla^2 \vec{E}(x,y,z,t) - \mu_0 \epsilon_0 \frac{\partial^2 \vec{E}(x,y,z,t)}{\partial t^2} = 0 \tag{1.2}$$

The wave equation may be decomposed into a continuum of linearly independent sinusoids through the Fourier transform; that is, each field can be expressed as $\vec{F}(x,y,z,t) = Re[\vec{F}(x,y,z)\exp(-i\omega t)]$. With this method, Maxwell's equations can be reduced to a spatial set of differential equations known as the time harmonic Maxwell's equations. Time dependant fields can then be constructed from the resulting basis set of linearly independent components [8]. Substituting the time harmonic form for the electric field into (1.2), we arrive at the Helmholtz equation, which is the time-independent form of the wave equation.

$$\nabla^2 \vec{E}(x,y,z) + k^2 \vec{E}(x,y,z) = 0 \tag{1.3}$$

Here, $k = \omega\sqrt{\mu_0\epsilon_0} = 2\pi/\lambda$ is known as the wavenumber. The first term that appears in (1.3) represents the curvature of $E(x,y,z)$ and describes the process of diffraction.

1.3 The scalar paraxial wave equation

The Helmholtz equation describes the time-independent propagation of radiation. However, this partial differential equation often proves difficult to solve or numerically compute. Fortunately, an approximation can be made which allows for easier computation while still capturing most of the dynamics of the Helmholtz equation. The approximation, called the slow varying envelope approximation (SVEA) assumes that the electric field can be described as the product of a rapidly varying beam phase and a slow varying beam amplitude profile which is expressed as $E(x,y,z) = \psi(x,y,z)\exp(ikz)$. Substitution into (1.3) and neglecting the minuscule term $\partial^2\psi(x,y,z)/\partial z^2$ gives:

$$i\frac{\partial\psi(x,y,z)}{\partial z} + \frac{1}{2k}\nabla_\perp^2\psi(x,y,z) = 0 \tag{1.4}$$

Where $\nabla_\perp^2$ is the transverse Laplacian. It should be noted that by invoking the SVEA another assumption has been implicitly made called the paraxial or “small angle" approximation [6]. This assumption assumes that the radiation propagates mostly in the $\hat{z}$ direction and is valid when $k_\perp/k = \sin(\theta) \approx \theta$.

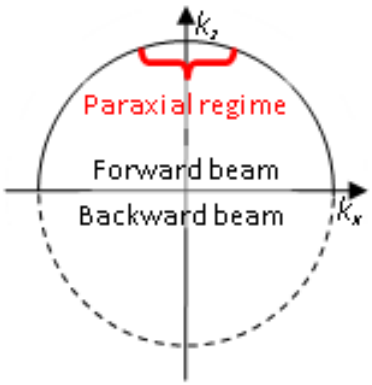

(a)

Figure 1.1: The paraxial regime assumes that radiation propagates mostly in the $\hat{z}$ direction. Graphic taken from [9].

1.4 Gaussian beam diffraction

In order to say that radiation like Bessel and Airy beams are special, they need to be compared to a common well understood wavefront. The standard textbook profile is the Gaussian beam. In order to characterize the evolution dynamics, one assumes a Gaussian wavefront with the form $\psi(r, z=0) = \psi_0 \exp[-i(P(z) + (k_0 n r^2)/2q(z))]$. Here, ψ_0 is the maximum envelope amplitude, n is the refractive index of the medium, $k_0 = \omega/c$, $\exp(-iP(z)) = q(0)/q(z)$ and $q(z) = z + iz_0$. The parameter $z_0 = k_0 n w_0^2/2$ is known as the Rayleigh length and is the distance the Gaussian beam propagates until its beam radius has reached $w(z) = \sqrt{2}w_0$. Finally, the value w_0 is known as the beam waist and is the minimum radius of the Gaussian beam which occurs at $z = 0$. With the above anstanz as an initial condition to (1.4), it can be shown that the following expression is satisfactory for all propagation distances [10]:

$$E(r,z) = \psi_0 \frac{w(0)}{w(z)} \exp\left[-\frac{r^2}{w^2(z)}\right] \exp\left[i\frac{k_0 n r^2}{2R(z)}\right] \exp\left[-i \arctan\frac{z}{z_0}\right] \exp\left[k_0 n z\right] \tag{1.5}$$

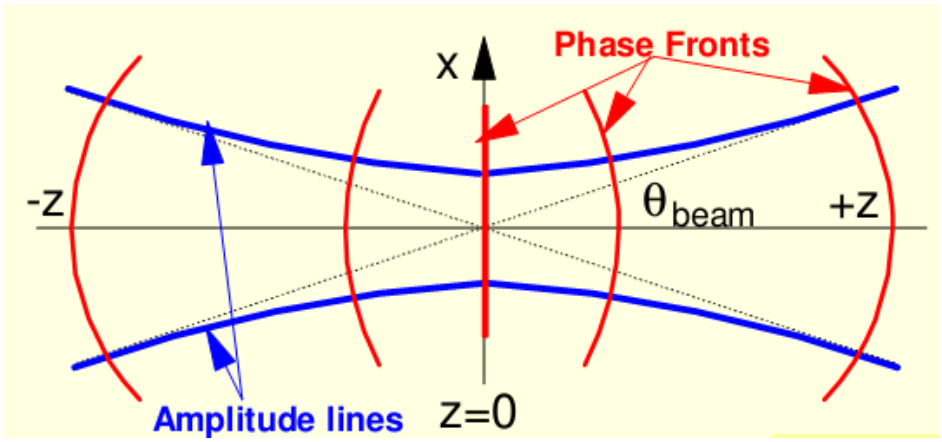

(a)

Figure 1.2: Gaussian beam propagation [10]

Where $w(z) = w_0\sqrt{1+(z^2/z_0^2)}$ and $R(z) = z(1+z_0^2/z^2)$. In our study of these more exotic beams, we will compare their behavior to the propagation dynamics of a Gaussian beam given by (1.5).

Chapter 2

The Bessel beam

2.1 Inception of the Bessel beam

The mathematical construct of the Bessel beam was first proposed in 1987 by Durnin [11] who was reviewing solutions to the Helmholtz equation published by Edmund Whittaker in 1902 [12]. The solution began by casting the Helmholtz equation (1.3) in cylindrical coordinates:

$$\frac{\partial^2 E(r,\theta,z)}{\partial r^2}+\frac{1}{r}\frac{\partial E(r,\theta,z)}{\partial r}+\frac{1}{r^2}\frac{\partial^2 E(r,\theta,z)}{\partial \theta^2}+\frac{\partial^2 E(r,\theta,z)}{\partial z^2}+k^2E(r,\theta,z) \quad (2.1)$$

Here, $r^2 = x^2 + y^2$ is the radial component in the transverse plane and $\theta = \arctan(y/x)$. The next important step is to assume a separable solution of the form $E(r,\theta,z) = R(r)\exp(in\theta)\exp(i\beta z)$, where β is a constant and n is an integer. Substitution of this into (2.1) results in Bessel's differential equation for the radial function:

$$r^2\frac{\partial^2 R(r)}{\partial r^2}+r\frac{\partial R(r)}{\partial r}+\left[\left(k^2-\beta^2\right)r^2-n^2\right]R(r)=0 \quad (2.2)$$

The linear combination of the two solutions to this second order differential equation is $R(r) = A_0J_n(\alpha r) + B_0Y_n(\alpha r)$ [13], where $\alpha^2 = k^2 - \beta^2$. Because of the singularity that $Y_n(\alpha r)$ has at $r = 0$, it is discarded giving a full complex electric field of:

$$E(r,\theta,z) = A_0 J_n(\alpha r)\exp(in\theta)\exp\left(i\beta z\right) \tag{2.3}$$

The electromagnetic field in (2.3) was termed the Bessel beam. A short while after, Durnin and two of his colleges published instructions for producing the first order Bessel radiation pattern along with experimental results which confirmed the existence of the beam 2.1 [1].

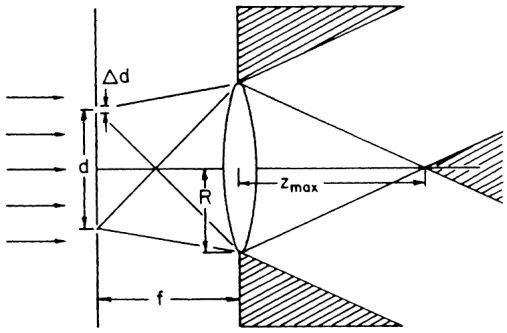

(a)

Figure 2.1: Experimental setup used by Durnin, Miceli, and Eberly [1].

2.2 The diffractionless property of the Bessel beam

Perhaps the most intriguing property of the Bessel beam is that the transverse intensity remains invariant upon propagation [1, 11]. The time averaged intensity of a beam is proportional to the absolute square of the electric field, $I \propto |E|^2$. Because the z dependence exists exclusively as a phase component in (2.3), it will vanish when considering the intensity profile.

$$I(r,\theta,z=0) = A_0^2 J_n^2(\alpha r) = I(r,\theta,z>0) \tag{2.4}$$

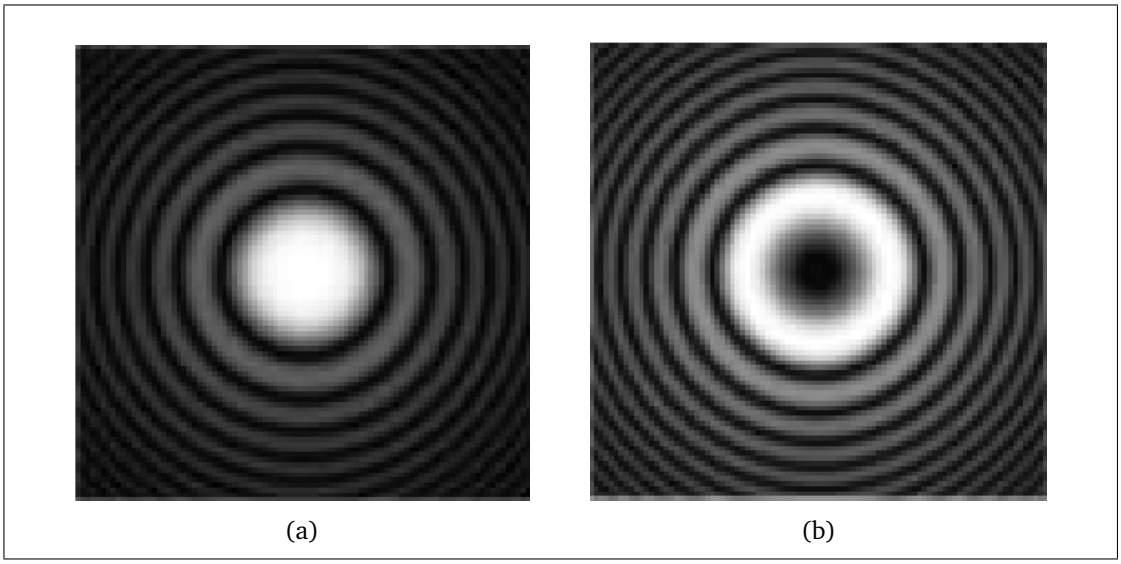

Figure 2.2: Example transverse intensity profiles of a) J_0 and b) J_1 Bessel beam.

Consequently, Bessel beams of all orders, n, are diffractionless, azimuthally symmetric, and consist of rings whose intensity maxima correspond to $J_n^2(\alpha r)$ 2.2.
The claim of that a wavefront could exhibit no diffraction stirred controversy at first. Skeptics objected that the center maximum of the J_0 beam was actually both an example of Poisson's spot and a line image resulting from the circular aperture used in Durnin's experiment 2.1 [14, 15]. Others argued that conventional Gaussian beams, which do not carry the diffractionless property, performed equally as well under a clearly fair comparison [16]. Durnin and his colleges responded that there are many ways to produce line images and these methods do not necessarily have the properties seen in the Bessel beam [17]. Furthermore, they reaffirmed that they "had [only] observed beams whose central maxima are remarkably resistant to the diffractive spreading commonly associated with all wave propagation" [18]. As a follow up to this scrutiny, Durnin, Miceli, and Eberly published a fair comparison between the properties of a Gaussian and a J_0 Bessel beam, mainly showing that the J_0 beam's first maximum had virtually no spreading at the Gaussian beam's Rayleigh length for the same FWHM [19].

2.3 Conical superposition

(a)

Figure 2.3: The Fourier spectrum of a Bessel beam is a ring in k-space [7].

The Bessel beam can be considered as the superposition of all plane waves propagating on a cone which is to say that the Fourier transform of a Bessel beam is a ring in k-space 2.3 [7]. Why is this so? To answer this question, we must make use of the paraxial wave equation in $1D$. We then guess a simple diffraction-free solution for the electric field envelope, $\psi(x,y,z) = \exp(i\alpha^2 z/2k)\cos(\alpha x)$, which upon inspection, is shown to satisfy (1.4). Here, $\alpha^2 = k_x^2 + k_y^2$.
This solution represents a pair of plane waves having: 1. k vectors of equal magnitude, 2. identical components along the $\hat{z}$ direction, and 3. equal and opposite components along the $\hat{x}$ direction (in general one plane wave in an arbitrary $\hat{\theta}$ direction emanating with equal ϕ is a solution - see 2.4). For our example, however, the resulting transverse intensity profile is a cosine-squared interference pattern.

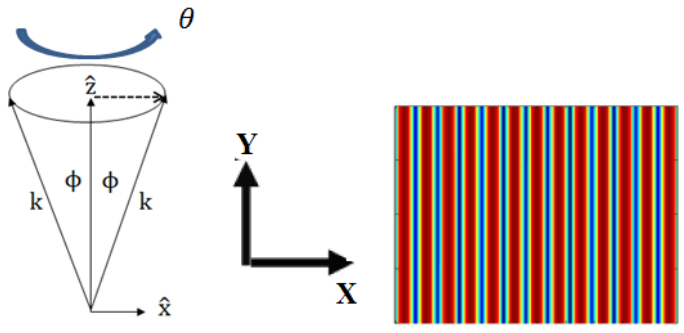

(a) (b)

Figure 2.4: a) The superposition of a pair of plane waves as shown results in a b) cosine-squared transverse intensity profile. Note that any emanating plane wave on this cone is a valid solution

The solution that gave rise to the diffractionless pattern shown in 2.4b had no constraint on the azimuthal orientation of the pair of plane waves, represented by θ. This free parameter offers a versatility if we now consider the $2D$ paraxial wave equation. Any single plane wave (it need not be a pair) holding the three properties defined previously can be arbitrarily oriented along θ and still satisfy (1.4). More importantly, any superposition of these diffractionless solutions will be a new diffractionless solution, leading to an infinite amount of diffractionless beam possibilities. An arbitrary superposition of these “conical plane waves" can be expressed by the following integral:

$$\psi(x,y,z) = \int_{-\pi}^{\pi} G(\theta) \exp\left(\frac{i\alpha^2}{2k}\right) \exp\left[i\alpha\left(x\cos\theta + y\sin\theta\right)\right] \mathrm{d}\theta \tag{2.5}$$

Where $G(\theta)$ is an arbitrary complex function which defines the arrangement of the conical plane waves. Being able to experimentally manipulate equation (2.5) could open possibilities for custom diffractionless beams. Some realizations of conical superposition are displayed in 2.5. The specific case of the Bessel beam can be interpreted as the superposition of these conical plane waves covering every azimuthal angle; that is, $G(\theta) = 1$ (see 2.5e). Because Bessel beams can be constructed this way, it follows that the zeroes of the beam have a π phase shift between adjacent rings [20].

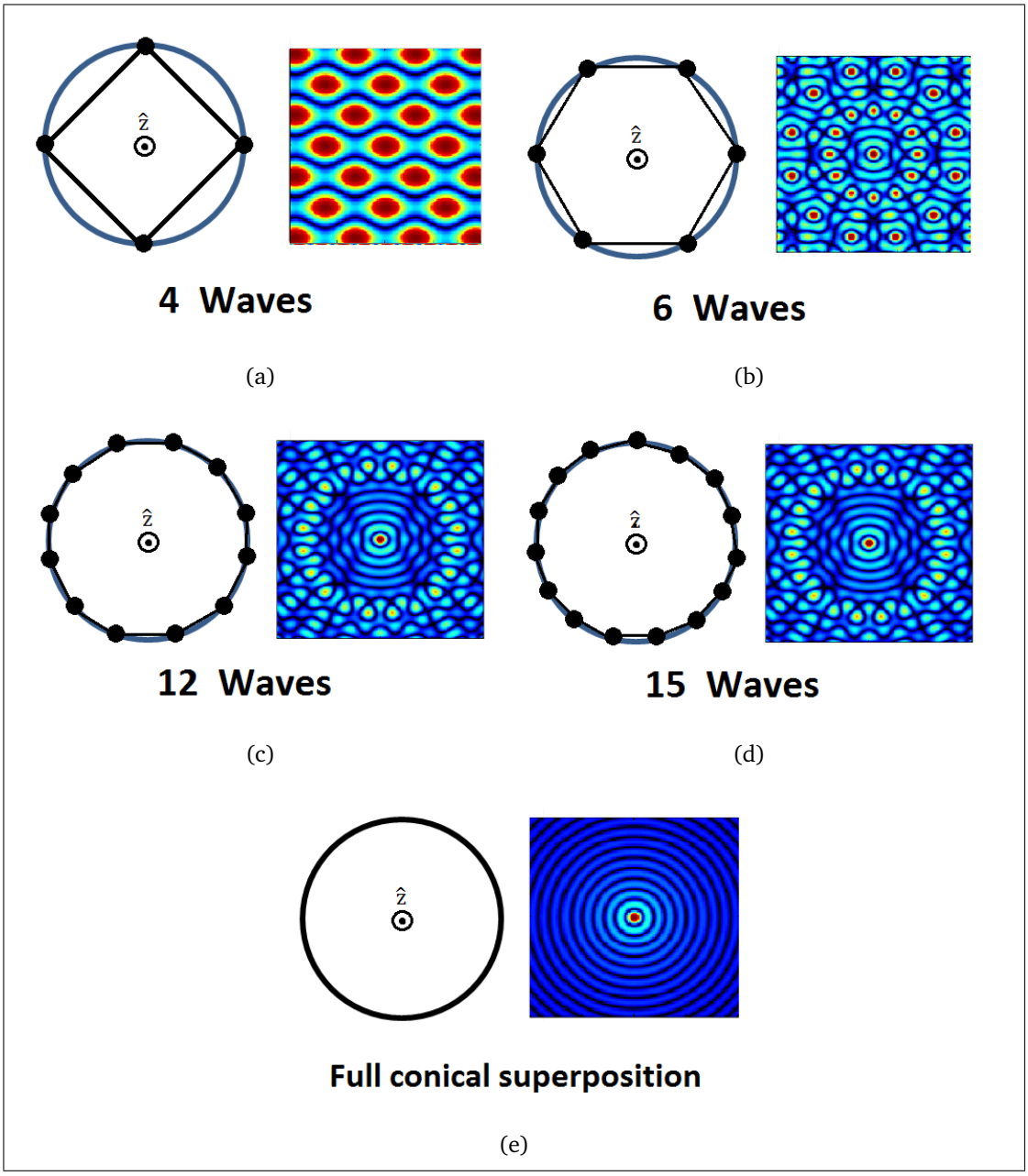

Figure 2.5: Superposition of conical plane waves result in diffractionless beams. In each picture, a black dot indicates the position of a single plane wave on the base of a cone. This is alongside the resulting transverse intensity profile for each.

2.4 Self-healing property of Bessel beams

Another property of the Bessel beam is its self-healing property [21]. Analogous to a starfish or lizard that can completely regenerate body parts, the Bessel beam has the ability to renew portions of its electric field which have been removed. The application of Babinet's principle explains this interesting property [22]. One knows that the complex amplitude of an unadulterated Bessel beam, E_{Bess}, follows (2.3) for $z \geq 0$. We then assume that an obstacle blocks portions of the Bessel beam at $z = 0$. This obstacle, if it were an aperture, would evolve a complex amplitude, E_Obs, which would be describable by the Fresnel diffraction integral.

$$E_{obs}(x,y,z) = \frac{\exp(ikz)}{i\lambda z} \times \int_{-\infty}^{\infty}\int_{-\infty}^{\infty} E_{obs}(x',y',z=0)\exp\left[\frac{ik}{2z}\left((x-x')^2+(y-y')^2\right)\right]\mathrm{d}x'\mathrm{d}y' \tag{2.6}$$

According to Babinet's principle, the disturbed Bessel beam will have a complex electric field that is equal to the difference between the undisturbed Bessel beam's and the obstacle's diffraction pattern; that is, $E_{Disturb} = E_{Bess} - E_{Obs}$. The total time averaged intensity is given by $\left|E_{Disturb}\right|^2$ or:

$$I_{Disturb} = E_{Disturb}E^{\star}_{Disturb} = \left|E_{Bess}\right|^2 + \left|E_{Obs}\right|^2 - E_{Bess}E^{\star}_{Obs} - E_{Obs}E^{\star}_{Bess} \tag{2.7}$$

Equation (2.7) consists of four terms which combine to give the total intensity of the disturbed field; however, the term E_{Bess} which follows (2.3), is invariant under propagation while the complex amplitude of the obstacle, E_{obs}, decreases with a factor of $1/z$ as seen in (2.6). Thus in the limit that $z \to \infty$, the complex amplitude of the obstacle approaches zero. Under these conditions (2.7) becomes the intensity of the Bessel beam only and we see that the effects of the disturbance have been repaired.

To illustrate this self-healing property, a simulation is reported where the second and third ring of the J_0 Bessel beam is removed and allowed to propagate. This is then compared to an undisturbed Bessel beam 2.6. It should be noted that due to the finite window of the simulation, the Bessel beam will not exhibit perfect

diffractionless behavior - this is strictly a numerical artifact. Looking at both 2.6c and 2.6d one can see that by $z = 400m$ the two transverse beam profiles are nearly the same.

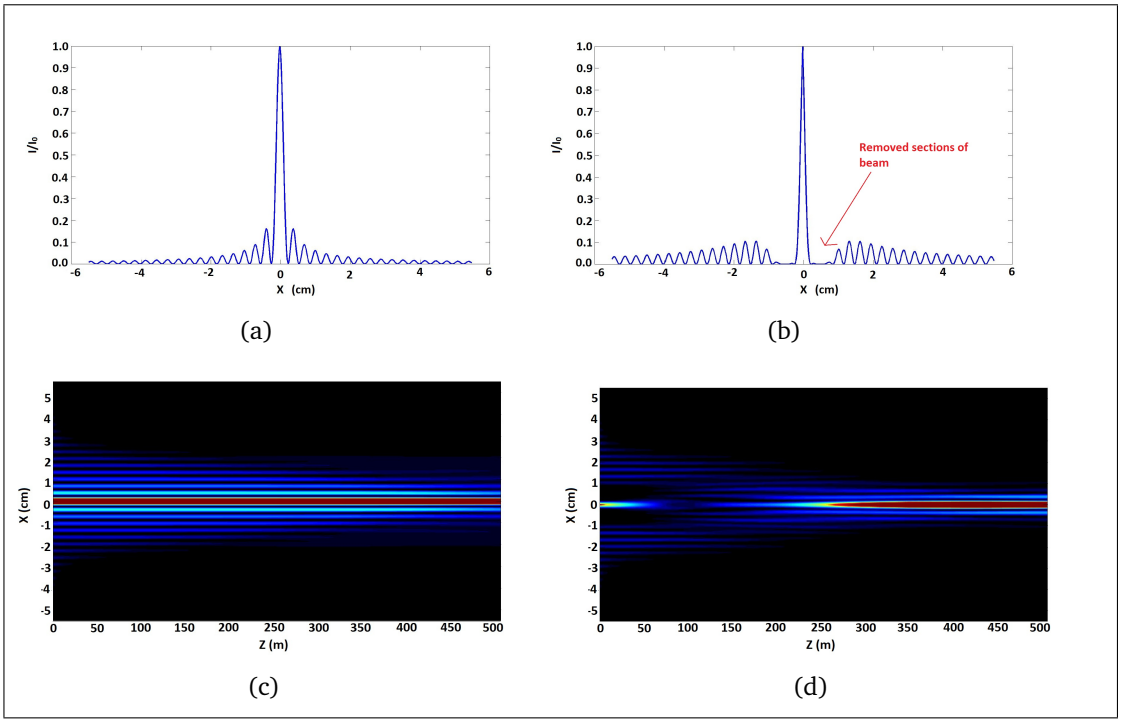

Figure 2.6: a) The initial profile of a J_0 Bessel beam along $Y = 0$. b) The initial profile of a J_0 Bessel beam along $Y = 0$ with the second and third ring removed. c) Side profile showing propagation of unadulterated Bessel beam. d) Side profile of the disturbed Bessel beam showing self-healing as $z \to \infty$

2.5 Finite power Bessel beams

In experimental practice, the complex field given in (2.3) cannot be produced. This is because a true Bessel beam is an ideal construct analogous to the plane wave, and like the plane wave, carries an infinite amount of power [23]. Realizing the importance of modeling a Bessel-like beam with a finite norm, Gori et al. introduced the Bessel-Gauss beam shortly after the introduction of the Bessel beam in 1987 [24]. This modification begins with a J_0 Bessel beam which has been apodized by a Gaussian profile:

$$\psi(r, z=0) = A_0 J_0(\alpha r) \exp\left(-r^2/w^2\right) \tag{2.8}$$

It can be shown that by using (2.8) as an initial condition to the paraxial wave equation, the following holds for all propagation distances:

$$\psi(r,z) = -\frac{ikA_0}{2zQ} \exp\left[ik\left(z + \frac{r^2}{2z}\right)\right] J_0\left(\frac{i\alpha kr}{2zQ}\right) \exp\left[-\frac{1}{4Q}\left(\alpha^2 + \frac{k^2 r^2}{z^2}\right)\right] \tag{2.9}$$

Where $Q = w^{-2} - ik/2z$. One of the ramifications of apodizing a Bessel beam is that its diffractionless property is compromised. This is apparent in the $1/z$ factor appearing in (2.9). However, the Bessel-Gauss beam still experiences smaller amounts of diffraction compared to a Gaussian beam of the same FWHM [19]. Because of this, the term quasi-diffractionless has been adopted. It is worth noting that quasi-diffractionless beams mostly retain their self-healing property as well, but in the limit of infinite propagation, their intensity approaches zero.

2.6 Efficient production of Bessel beams

The experimental procedure introduced by Durnin et al. [1] was done by allowing an incident plane wave to pass through a circular opening and then focused with a lens 2.1, a method that expanded off a similar procedure studied by John McLeod [25]. The idea is that the plane wave incident on the circular opening creates a ring of point sources. This is then focused with a lens which results in a scaled Fourier transform of the ring at focus. As stated earlier in section 2.3, the Fourier transform of a Bessel beam is a ring in k-space, therefore, this simple method produces a Bessel beam. Unfortunately, such a method is inefficient at collecting large amounts of light [26]. Furthermore, a circular aperture causes rapid on-axis intensity oscillations giving erratic intensity variations [7]. An optical element, called an axicon, can produce a Bessel beam and avoid these problems 4.9 [3, 7, 25, 26].

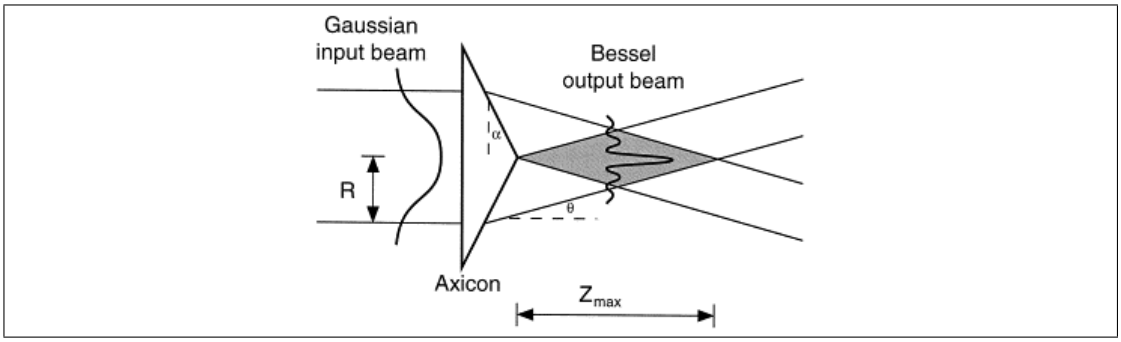

Figure 2.7: Axicon lens producing a Bessel beam [27]

It is worth noting that other methods exist which produce Bessel beams such as using a spatially filtered Fabry-Perot resonator [28] or a computer generated hologram [29]; however, the axicon lens remains the simplest and most efficient method [7].

Chapter 3

The Airy Beam

3.1 The inception of the $(1+1)D$ and $(2+1)D$ Airy beam

The origins of the Airy beam are rooted in quantum mechanics. In 1978, Berry and Balazs theoretically developed a unique solution to the Schrodinger equation which showed that a free accelerating particle could evolve [30]. Because of the isomorphism between the Schrodinger equation and the paraxial wave equation, Siviloglou and Christodoulides were able to greatly extend this idea into the field of optics where it flourished. They introduced the finite energy Airy beam by assuming an initial electric field envelope of the form: $\psi(s,\xi=0)=Ai(s)\exp(as)$ [2]. Here, a is a decay factor and $s=x/x_0$ and $\xi=z/kx_0^2$ are coordinates corresponding to a normalized version of the paraxial wave equation:

$$i\frac{\partial\psi(s,\xi)}{\partial\xi}+\frac{1}{2}\frac{\partial^2\psi(s,\xi)}{\partial\xi^2}=0 \tag{3.1}$$

The solution to (3.1) with the apodized Airy beam initial condition is given by [2]:

$$\psi(s,\xi)=Ai\left[s-\left(\frac{\xi}{2}\right)^2+ia\xi\right]\exp\left[as-\left(\frac{a\xi^2}{2}\right)-\left(\frac{i\xi^3}{12}\right)+\left(\frac{ia^2\xi}{2}\right)+\left(\frac{is\xi}{2}\right)\right] \tag{3.2}$$

The analytic solution given by (3.2) carries some of the intriguing characteris-

tics of the Bessel beam. For example, it exhibits its diffractionless [30] and self-healing properties [31]. However, it is unique because it is the only diffractionless $(1+1)D$[1]solution to the paraxial wave equation and cannot be constructed from the conical superposition of plane waves [32]. Lastly, it has the additional property of freely accelerating or bending which is discussed in the next section.

To demonstrate the quasi-diffractionless properties of the $(1+1)D$ finite Airy beam, assume the following parameters: $x_0 = 100\mu m$ and $\lambda = 500nm$. From this, we obtain a Gaussian Rayleigh range of $z_0 = kx_0^2 = 12.56cm$. This corresponds to a main airy lobe FWHM of $171\mu m$ which remains quasi-diffractionless upon propagation for roughly 6, 8, and 10 Gaussian Rayleigh ranges for $a = .10, .05, .01$ respectively. Fig. 4.10 contains plots which illustrate equation (3.2) for these values of a.
Airy beams in two dimensions can be represented as the product of two orthogonal one dimensional versions [2, 33]. Fig. 3.2 shows the transverse intensity of this profile for three different propagation distances and a constant apodization parameter of $a = .07$.

[1]The notation $(n+1)D$ refers to the n coordinates involved in addition to the propagating $\hat{z}$ direction

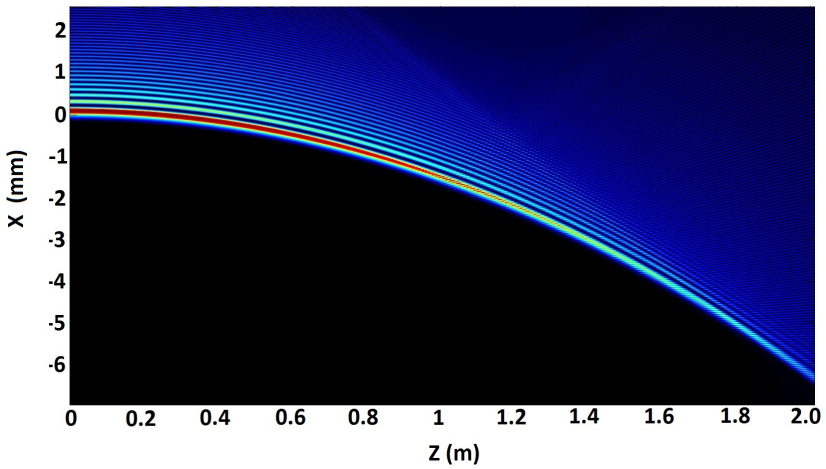

(a)

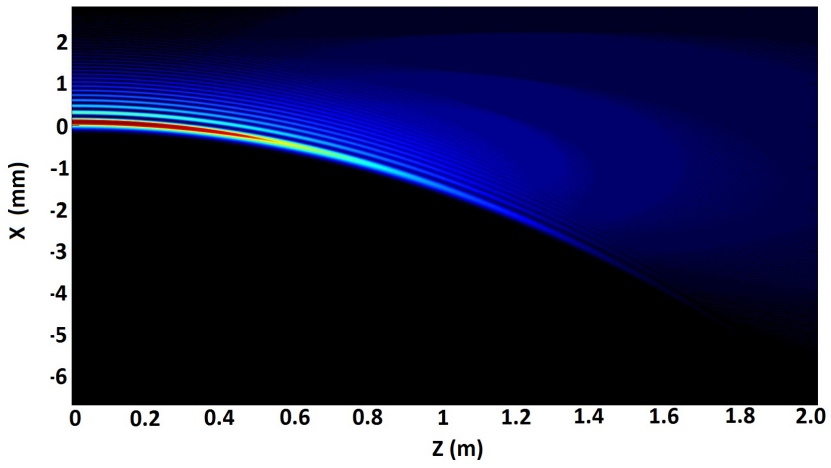

(b)

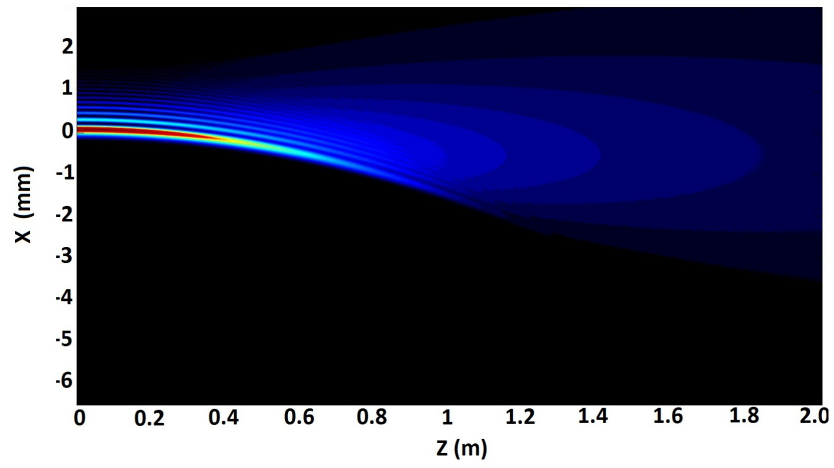

(c)

Figure 3.1: Propagation of a finite Airy beam with various decay parameters. a) decay of $a = .01$, b) decay of $a = .05$, c) decay of $a = .10$

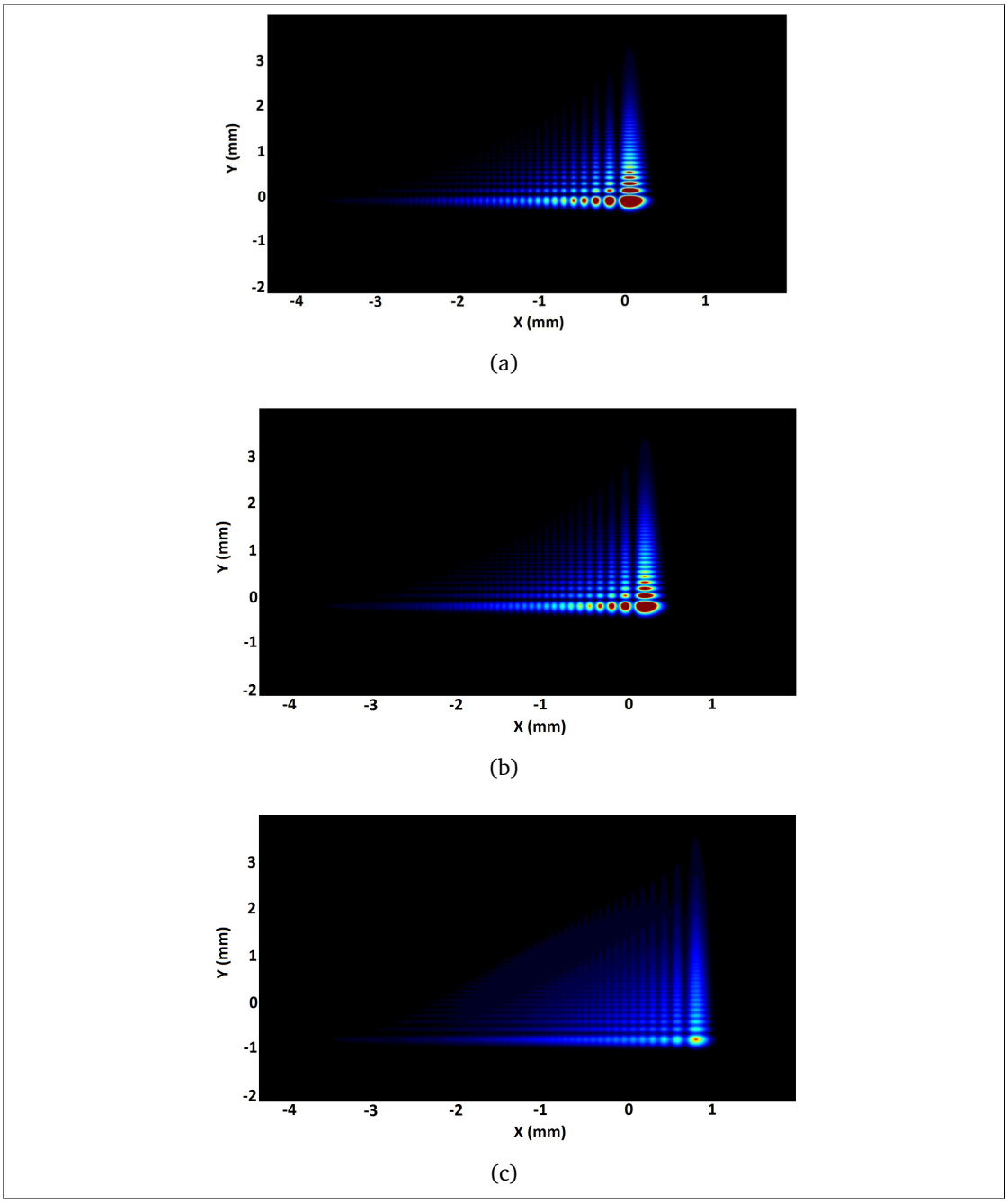

Figure 3.2: $2D$ transverse intensity profile of Airy beam at various propagation distances. a) $z = 0.00cm$, b) $z = 55.30cm$, c) $z = 75.40cm$

A few months after setting the theoretical framework of the Airy beam, Siviloglou et. al followed up with the experimental observation of both the $(1+1)D$ and

$(2+1)D$ Airy beams [34]. The method to realizing these wavefronts was similar to the approach discussed with the Bessel Beam 2.1. The k-space of the finite Airy beam, a Gaussian beam modulated with a cubic phase 3.3, was arranged using a spatial light modulator (SLM). Then, a convergent lens was used to focus the radiation, approximately creating the Fourier transform of the wavefront. In the case of the $(1+1)D$ beam, a cylindrical lens was used in order to focus in one dimension only. Note that the use of a phase mask to induce the cubic phase is an alternative method that will pass more light than a SLM.

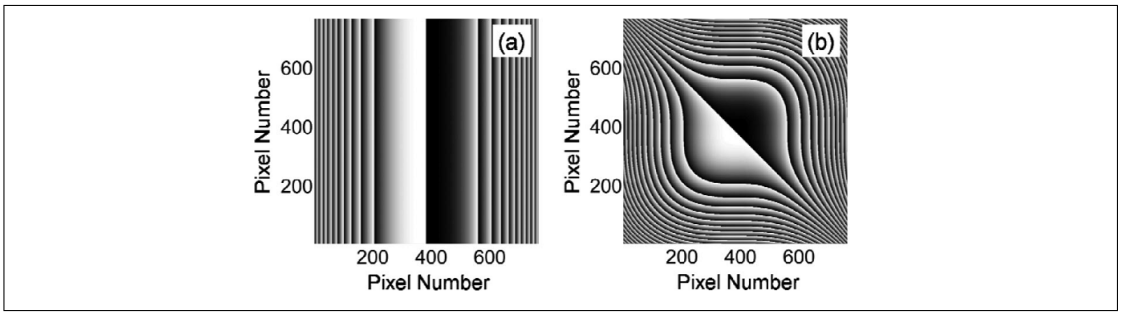

Figure 3.3: Phase masks used to apply a cubic phase modulation on a Gaussian beam. Left: $(1+1)D$ phase mask. Right: $(2+1)D$ phase mask. In each, black corresponds to zero phase shift and white to a 2π phase shift.

3.2 The freely accelerating property of the Airy beam

Airy beams are unique in the sense that they lack parity symmetry and tend to freely accelerate and bend during propagation even though no force acts upon it. This process is apparent in 4.10 and 3.2. Specifically in 3.2, the bending is illustrated by the diagonal movement of the main Airy lobe as it propagates. This unique property is elucidated on the basis of the equivalence principle which has been used to successfully explain other similar situations [35, 36]. One might also claim that this feature violates Ehrenfest's theorem. However, although the main features of the Airy profile are freely accelerating, the center of gravity of the entire profile moves with constant velocity [37].

Because of the $(\xi/2)^2$ term in (3.2), the Airy beam bends in a parabolic fashion and is akin to the projectile motions of an object under the influence of gravity [32]. By supposing an initial condition of the form $\psi(s,\xi=0)=Ai(s)\exp(as)\exp(ivs)$ and

applying (3.1), one can find a solution similar to (3.2) that contains the parameter v. This parameter is analogous to the initial launch angle of a projectile. Control over an Airy beam's launch angle could allow for the circumvention of objects (Fig. 12) [32]. Recently, the freely accelerating property of Airy beams has been utilized to realize curved ultraintense plasma channels in air [38]. This could offer new angles to remote spectroscopy, terahertz wave generation, and few cycle pulse compression [39, 40, 41, 42].

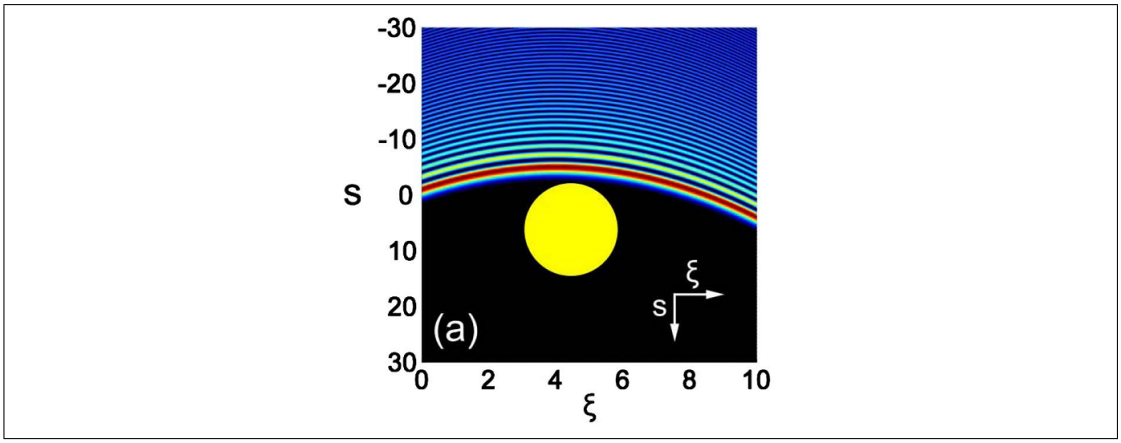

Figure 3.4: Controlling the initial angle of an Airy beam can be used to circumvent objects [32].

3.3 Autofocusing beams

One of the most important characteristics of optical beams is their focusing dynamics in free space; that is, how they collapse under linear conditions. A wavefront will focus or defocus depending on its initial phase and amplitude distribution. For example, in 1.2 we saw that a standard Gaussian wavefront has a complex electric field given by (1.5). The peak intensity of such a beam follows a Lorentzian distribution - a somewhat gently rising and falling function. However, in applications such as corneal refractive surgery [43] or optical filamentation [44], a beam which instead suddenly spikes in intensity and then subsides quickly is more desirable. A good candidate to meet these criteria is a radially symmetric arrangement of $(1+1)D$ Airy beams in free space [45]:

$$\psi(r, z=0) = Ai\left[r_0 - r\right] \exp\left[a\left(r_0 - r\right)\right] \tag{3.3}$$

Where r_0 is the initial radial displacement of the main ring. Note that for $r \leq r_0$ equation (3.3) decays exponentially and for $r \geq r_0$ the slowly decaying Airy oscillations occur. As an example, consider a case where $r_0 = 1cm$ and $a = .05mm^{-1}$ 3.5.

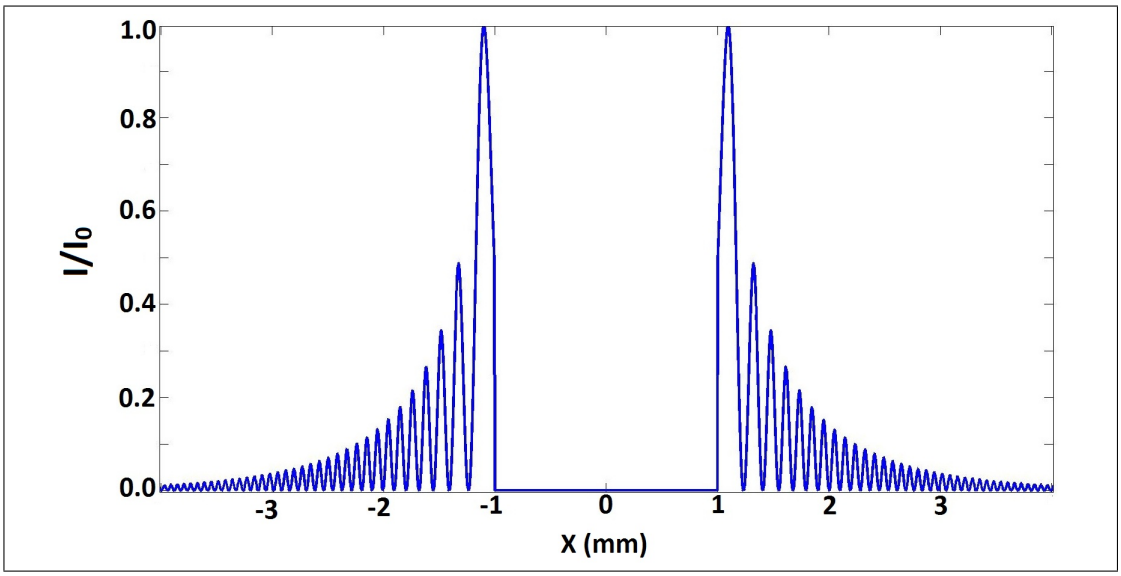

Figure 3.5: Initial intensity distribution of equation (3.3) along $Y = 0$ for $r_0 = 1cm$ and $a = .05mm^{-1}$. Values are scaled to an initial peak value of unity

The complex electric field envelope shown in 3.5 will evolve according to the Fresnel diffraction integral that was introduced in (2.6); however, this integral can be simplified because of the azimuthal symmetry of the circular Airy beam. The simplified integral is given by:

$$\psi(r,z) = \frac{1}{2\pi}\int_0^\infty \tilde{\psi}(k_r, z=0) k_r J_0(k_r r) \exp\left[-\frac{ik_r^2 z}{2}\right] \mathrm{d}k_r \tag{3.4}$$

Where $\tilde{\psi}(k_r, z=0)$ is the Hankel transform of (3.3)

$$\tilde{\psi}(k_r, z=0) = \int_0^\infty \psi(k_r, z=0) r J_0(k_r r) \mathrm{d}r \tag{3.5}$$

Numerical computation of $\psi(r,z)$ can be accomplished using a symmetric split-

step beam propagation method [46]. A cross section of the resulting propagation dynamics, illustrated in Fig. 3.6, has the following properties: 1. The center profile of the wavefront abruptly focuses to an intensity that is 120 times the initial peak intensity. 2. After coming to the sudden focus, the peak intensity drops off rapidly. 3. The focusing occurs in the absence of nonlinear effects. 4. After focusing, the far field diffraction pattern approximately forms a finite first order Bessel beam [47]. The form of the beam given by 3.3 can be generalized to include an entire family of abruptly autofocusing beams. These beams can be understood via the concept of caustics, and careful manipulation of their sub linear chirps allows for one to pre-engineer a wavefront resulting in customizable autofocusing characteristics [48].

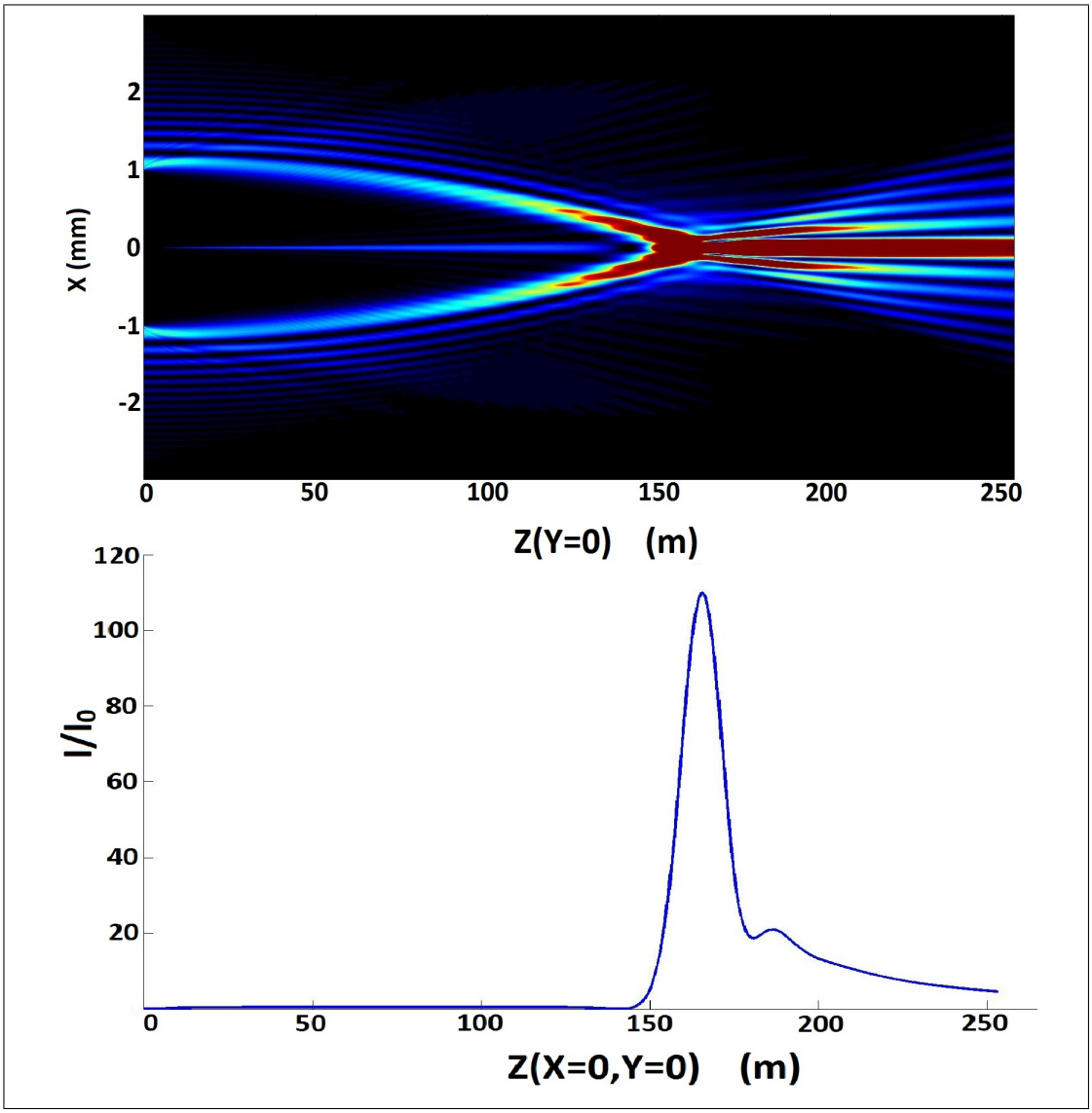

Figure 3.6: (Above) Cross section along $Y = 0$ showing the propagation dynamics of the radial Airy distribution given by (3.3). (Below) central intensity along $Y = X = 0$ shows the abruptly focusing characteristic of this wavefront. As before, intensity values are scaled to the initial peak intensity value

Chapter 4

Hydrogen-like symmetry bullets

4.1 Brief overview of spatio-temporal beams

In the spatio-temporal domain, the prospect for optical bullets that can simultaneously negotiate both dispersion and diffraction effects in the bulk has been actively pursued by several research groups in both the linear and nonlinear regimes [49, 50, 51]. In general, an optical wavepacket propagating in a homogeneous dielectric medium will expand because of diffraction effects while at the same time its temporal profile will broaden because of dispersion. In the linear domain, specific wave solutions are known to exist under normally and anomalously dispersive conditions. For normal dispersion, these solutions exhibit an X-wave structure [52, 53] - a direct outcome of the bidispersive nature of the underlying wave equation [54]. In the anomalous domain, spherical O-waves [51, 55] are allowed and Bessel-X pulses are possible under specific conditions [56]. Recently, 3D Airy-Bessel bullets that are impervious to both dispersion and diffraction have been suggested [2] and successfully demonstrated in dispersive media [57]. This versatile class of optical wavepackets was made possible by exploiting the fact that non-spreading Airy waves can exist even in one dimension. This class of Airy-Bessel bullets is possible irrespective of the dispersion properties of the material itself.

The quest for such spatio-temporal entities is clearly intertwined with experimental capabilities of simultaneously shaping their $\vec{k} - \omega$ spectra. Over the years, various techniques have been developed to address these needs in either the spatial or

temporal domain [58, 59]. Lately, methods that allow for the generation of quasi-nondiffracting light beams with complex transverse shapes have been suggested [60]. Further progress in this area may pave the way towards the generation of other exotic space-time bullets with unique properties tailored for particular light-matter interaction processes [61].

4.2 Problem Formulation and Analysis

In general, the primary electric field associated with a wavepacket can be expressed through a slowly varying envelope via $\vec{E}(\vec{r},t) = \hat{u}\psi(\vec{r},t)\exp\left(i\left(k_0 z - \omega_0 t\right)\right)$ where ω_0 is the carrier angular frequency, $k_0 = \omega_0 n(\omega_0)/c$, is the wavenumber evaluated at ω_0, and $n(\omega_0)$ is the refractive index. The spatio-temporal evolution of the envelope, $\psi(\vec{r},t)$, under the combined action of diffraction and group velocity dispersion is known to obey the following evolution equation:

$$i\frac{\partial\psi}{\partial z} + \frac{1}{2k}\left(\frac{\partial^2\psi}{\partial x^2} + \frac{\partial^2\psi}{\partial y^2}\right) - \frac{k_2}{2}\frac{\partial^2\psi}{\partial\tau^2} = 0 \tag{4.1}$$

where in (4.1), $\tau = t - z/v_g$ is a time coordinate frame moving at the wave's group speed, v_g, and $k_2 = \partial^2 k/\partial\omega^2$ represents the dispersive coefficient of the homogeneous medium again evaluated at ω_0. The material is anomalously dispersive if $k_2 < 0$ and is normal if $k_2 > 0$. The transverse spatial operators in (4.1) account for diffraction effects while the temporal operator for the action of dispersion. Equation (4.1) can be judiciously scaled by normalizing the independent variables involved in such a way that the diffraction length $L_{diff} = 2kd^2$ is equal to the corresponding dispersion length $L_{disp} = \tau_0^2/\left|k_2\right|$, i.e., $L_{disp} = L_{diff}$. Here, d is an arbitrary length scale and τ_0 is associated with the pulsewidth of the wavepacket. From this point on, the material dispersion is taken to be anomalous in our analysis. Under these assumptions, Eq. (4.1) takes the form:

$$i\frac{\partial\psi}{\partial Z} + \frac{\partial^2\psi}{\partial X^2} + \frac{\partial^2\psi}{\partial Y^2} + \frac{\partial^2\psi}{\partial T^2} = 0 \tag{4.2}$$

where in (4.2) we have employed the following set of normalized coordinates and variables $X = x/d$, $Y = y/d$, $Z = z/\left(2kd^2\right)$, and $T = \tau/\tau_0$.

The aforementioned spatio-temporal wavepackets can be studied experimentally in anomalously dispersive bulk media such as silica glass. Silica, at $\lambda_0 = 1550nm$, exhibits a dispersive coefficient of $k_2 = -2.8 \times 10^{-2} ps^2/m$. For this example, such a dispersion-diffraction equalization ($L_{diff} = L_{disp} = 5.7cm$) is possible provided that the wavepacket is generated from a transform limited femtosecond laser has the following parameters: $\tau_0 = 40fs$, $d = 100\mu m$. In what follows, we will derive the electromagnetic equations describing the internal power flow associated with a spatio-temporal wavepacket as a result of dispersion and diffraction. This is necessary in order to comprehend the underlying dynamics in such systems. With this in mind, we employ a perturbative approach, valid within the slowly varying envelope approximation and paraxial diffraction optics. We start our analysis by writing the electric field as a superposition of plane waves centered around a carrier frequency, ω_0. Without any loss of generality, the primary electric field component is taken here to be $\hat{x}$ polarized. In this case:

$$\vec{E} = \hat{x} \iiint F_0 \left(\omega - \omega_0; k_x, k_y\right) \exp\left[i\left(\vec{k}\cdot\vec{r} - \omega t\right)\right] \mathrm{d}\omega \mathrm{d}k_x \mathrm{d}k_y \tag{4.3}$$

This same field can also be expressed in terms of a slowly varying envelope ψ, i.e. $\vec{E}(\vec{r},t) = \hat{x}\psi(\vec{r},t)\exp\left[i\left(k_0 z - \omega_0 t\right)\right]$. Given that $k_z \approx k - \left(k_x^2 + k_y^2\right)/(2k)$ and that the wavenumber can be expanded in a Taylor series around ω_0, $k \approx k_0 + k_1\Omega + k_2\Omega^2/2$ (where $\Omega = \omega - \omega_0$), one finds:

$$\begin{aligned}\psi(\vec{r},t) = \iiint & F_0\left(\Omega; k_x, k_y\right) \exp\left[i\left(k_x x + k_y y\right)\right] \\ & \times \exp\left[-\frac{i}{2k}\left(k_x^2 + k_y^2\right) z\right] \exp\left[i\left(k_1\Omega + k_2\frac{\Omega^2}{2}\right) z\right] \\ & \times \exp\left[-i\Omega\tau\right] \mathrm{d}\,\Omega\, \mathrm{d}\,k_x\, \mathrm{d}\,k_y\end{aligned} \tag{4.4}$$

where $v_g^{-1} = k_1$. The associated longitudinal component of the electric field can be then obtained from $\nabla\cdot\vec{E} = 0$, leading to a total (corrected to first order) electric field that is given by:

$$\vec{E} = \left(\hat{x}\psi + \hat{z}\frac{i}{k_0}\frac{\partial \psi}{\partial x} \right) \exp\left[i\left(k_0 z - \omega_0 t \right) \right] \tag{4.5}$$

The primary magnetic field of this wavepacket can be obtained from the electric field through the material intrinsic impedance $\eta(\omega) = \eta_0 / n(\omega)$ where $\eta_0 = \sqrt{(\mu_0/\epsilon_0)}$. Therefore:

$$\begin{aligned}
\vec{H} &= \hat{y} \iiint \frac{F_0\left(\Omega; k_x, k_y\right)}{\eta(\omega)} \\
&\quad \times \exp\left[i\left(\vec{k}\cdot\vec{r} - \omega t \right) \right] \mathrm{d}\,\omega\, \mathrm{d}\,k_x\, \mathrm{d}\,k_y \\
&= \hat{y} \iiint \frac{F_0\left(\Omega; k_x, k_y\right)}{\eta_0} \left(n_0 + n_1 \Omega \right) \exp\left[i\left(k_x x + k_y y \right) \right] \\
&\quad \times \exp\left[-\frac{i}{2k}\left(k_x^2 + k_y^2 \right) z \right] \exp\left[i\left(k_1 \Omega + k_2 \frac{\Omega^2}{2} \right) z \right] \\
&\quad \times \exp\left[-i\Omega\tau \right] \mathrm{d}\,\Omega\, \mathrm{d}\,k_x\, \mathrm{d}\,k_y \exp\left[i\left(k_0 z - \omega_0 t \right) \right] \\
&= \frac{1}{\eta_0}\hat{y} \left[n_0 \psi + i n_1 \frac{\partial \psi}{\partial \tau} \right] \exp\left[i\left(k_0 z - \omega_0 t \right) \right]
\end{aligned} \tag{4.6}$$

where in (4.13) $n(\omega) = n(\omega_0 + \Omega)$ and $n_1 = \partial n / \partial \omega$ at ω_0. These coefficients can in principle be evaluated from the corresponding Sellmeier equation associated with the dispersive medium. From $\nabla \cdot \vec{H} = 0$, one can determine (to first order) the longitudinal component of the magnetic field. The total magnetic field is found to be:

$$\vec{H} = \left(\frac{1}{\eta_0}\hat{y} \left[n_0 \psi + i n_1 \frac{\partial \psi}{\partial \tau} \right] + \hat{z} i \frac{n_0}{k_0 \eta_0}\frac{\partial \psi}{\partial y} \right) \exp\left[i\left(k_0 z - \omega_0 t \right) \right] \tag{4.7}$$

The power flow within the spatio-temporal wavepacket can now be established from Eqs. (4.12) and(4.14), i.e.

$$\overrightarrow{S_{av}} = \hat{z}\frac{n_0}{2\eta_0}\left|\psi\right|^2 - i\hat{z}\frac{n_1}{4\eta_0}\left[\psi\frac{\partial\psi^\star}{\partial\tau} - \psi^\star\frac{\partial\psi}{\partial\tau}\right] + \frac{in_0}{4k_0\eta_0}\left[\psi\nabla_\perp\psi^\star - \psi^\star\nabla_\perp\psi\right] \quad (4.8)$$

where $\nabla_\perp = (\partial^2/\partial x^2)\hat{x} + (\partial^2/\partial y^2)\hat{y}$. The last two terms in Eq. (4.15) correspond to the relative power flow corrections. The second term along $\hat{z}$ is due to temporal effects while the $\nabla_\perp$ component accounts for the energy transport because of transverse effects. We note here that the first term in (4.15) represents the dominant contribution to the power flow. Equation (4.15) can now be expressed in normalized units as follows:

$$\begin{aligned}
\overrightarrow{S_{av}} &= \overrightarrow{S_0} + \overrightarrow{S_r} \\
\overrightarrow{S_0} &= \hat{z}\frac{n_0}{2\eta_0}\left|\psi\right|^2 \\
\overrightarrow{S_r} &= -i\hat{z}\frac{n_1}{4\eta_0\tau_0}\left[\psi\frac{\partial\psi^\star}{\partial T} - \psi^\star\frac{\partial\psi}{\partial T}\right] + \\
&\quad \frac{in_0}{4k_0\eta_0 d}\left[\psi\tilde{\nabla}_\perp\psi^\star - \psi^\star\tilde{\nabla}_\perp\psi\right]
\end{aligned} \quad (4.9)$$

where the transverse $\tilde{\nabla}_\perp$ operator involves the X and Y scaled coordinates .

4.3 Optical bullets with hydrogen-like symmetries

Propagation invariant solutions to Eq. (4.2) can be directly obtained via separation of variables in spatio-temporal spherical coordinates R, θ, ϕ where $R^2 = X^2 + Y^2 + T^2$. To do so, we write the solution as $\psi = \psi_0 G(R)P(\theta)\exp\left(im\phi\right)\exp\left(-i\alpha^2 Z\right)$. Direct substitution of this latter form into (4.2) gives the following equations:

$$\frac{d}{d\theta}\left[\sin\theta\frac{dP}{d\theta}\right] + \sin\theta\left[\ell\left(\ell+1\right) - \frac{m^2}{\sin^2\theta}\right]P = 0 \quad (4.10)$$

$$R^2\frac{d^2G}{dR^2}+2R\frac{dG}{dR}+\left(\alpha^2R^2-\ell\left(\ell+1\right)\right)G=0 \tag{4.11}$$

It is interesting to note that similar differential equations are encountered in the analysis of hydrogen quantum orbitals. The solutions to the Legendre equation (4.10) can be obtained in terms of the associated Legendre polynomials, $P_\ell^m(\gamma)$, of degree ℓ and order m where $\gamma=\cos\theta$. Equation (4.11) on the other hand has spherical Bessel function solutions $j_\ell(\alpha R)=\sqrt{\pi/(2\alpha R)}J_{\ell+1/2}(\alpha R)$ which can be expressed in terms of elementary functions since ℓ belongs to the natural numbers. Therefore, invariant solutions to Eq. (4.2) are given by:

$$\psi=\sqrt{2\pi}\psi_0 j_\ell(\alpha R)P_\ell^m(\cos\theta)\exp\left[im\phi\right]\exp\left[-i\alpha^2Z\right] \tag{4.12}$$

As indicated above, the integer index ℓ takes values from the set $\ell=0,1,2,...$ while the integer order m is constrained in the range $|m|\leq\ell$. We note that in general these solutions depend on how the spherical coordinate system is oriented with respect to the X,Y,T axes. If for example, the T coordinate coincides with the spherical polar axis then $\theta=\arctan(\sqrt{X^2+Y^2}/T)$ and $\phi=\arctan(Y/X)$. In principle, however, the spherical polar axis can be oriented in any direction (for example along X or Y). This choice has an important effect on the associated relative internal power flows $\vec{S_r}$. In this case, the vorticity arising from the term $\exp\left[im\phi\right]$ takes on a whole new physical meaning in space-time.

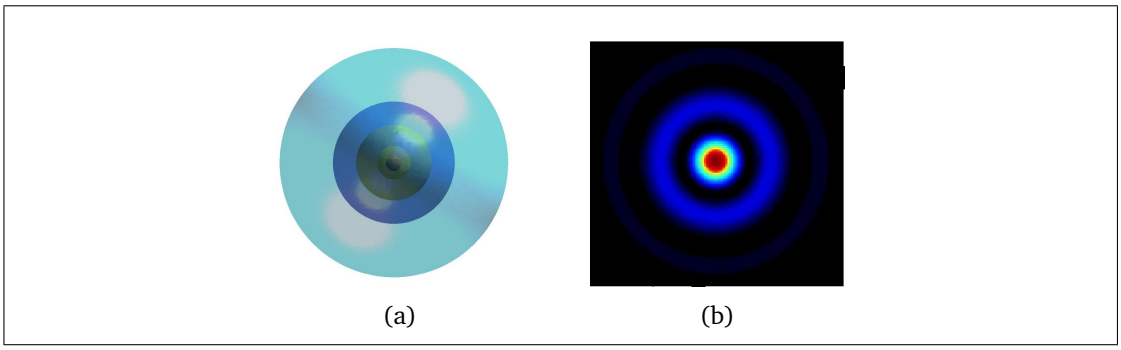

(a) (b)

Figure 4.1: (a) Intensity iso-surface plots of an $\ell=m=0$ optical bullet. (b) Intensity cross section reveals the $j_0(R)\propto\sin R/R$ profile of this 's' state.

The simplest possible member in this family of solutions given by Eq. (4.12) is obtained when $\ell=m=0$. This lowest state optical bullet has no internal spin

and because it is like hydrogen's 's' orbital we call it an 's' bullet. An iso-intensity contour plot of this wavepacket is depicted in Fig. 4.1a. This wave is evidently spherical and its field follows a $j_0(R) \propto \sin R/R$ radial distribution. As a result, its intensity structure involves concentric spherical shells as shown in Fig 4.1b which represents a cross-section of this bullet in the $Y-T$ plane. We note that this specific 's' member is identical to the so-called "o-wave" previously obtained in other studies [51, 55]. Figure 4.2a, on the other hand, shows an iso-intensity plot of a space-time optical bullet when $\ell = 1, m = 0$, in which case it corresponds to a p_T-like orbital. The structure of this solution is no longer spherical and lacks spin since $m = 0$. Note that this same state can be arbitrarily oriented in the X, Y, T system. A cross-section of this solution at $X = 0$ (Fig. 4.2b) reveals the finer structure in its field distribution.

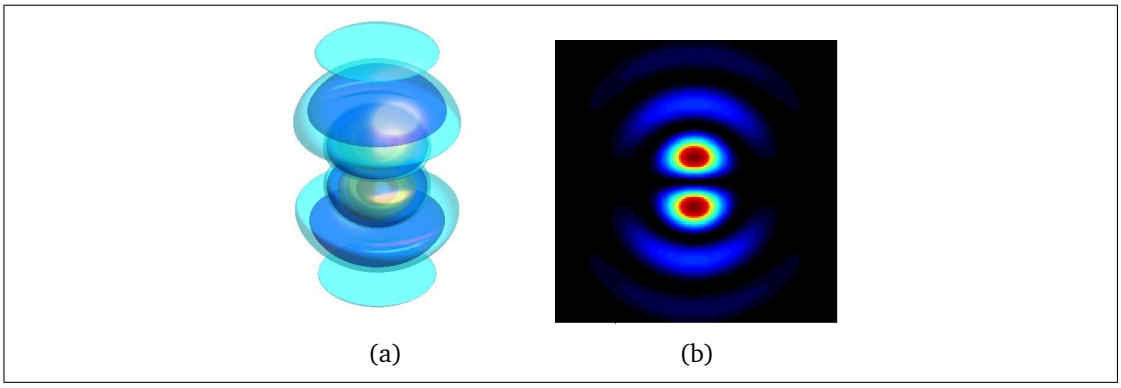

(a) (b)

Figure 4.2: (a) Intensity iso-surface plots of an $\ell = 1, m = 0$ optical bullet. (b) Intensity cross section of 'p' shell for X=0.

As in the case of 's'-bullets these solutions exhibit infinitely many rings in sharp contrast to the quantum orbitals of hydrogen. This is because in our case the Coulombic potential is not involved. Similarly, p_x and p_y bullets can be generated from the same "quantum" numbers $\ell = 1, m = 0$. By further increasing the ℓ number, optical bullets of higher symmetries can be generated similar to the ones depicted in Fig 3. In particular, when $\ell = 2$ and $m = 0$ (Fig. 4.3a) the propagation invariant wavepacket corresponds to the d_{TT} group (d-orbitals). Similarly, an f-symmetric light bullet with $\ell = 3, m = 0$ is shown in Fig. 4.3b.

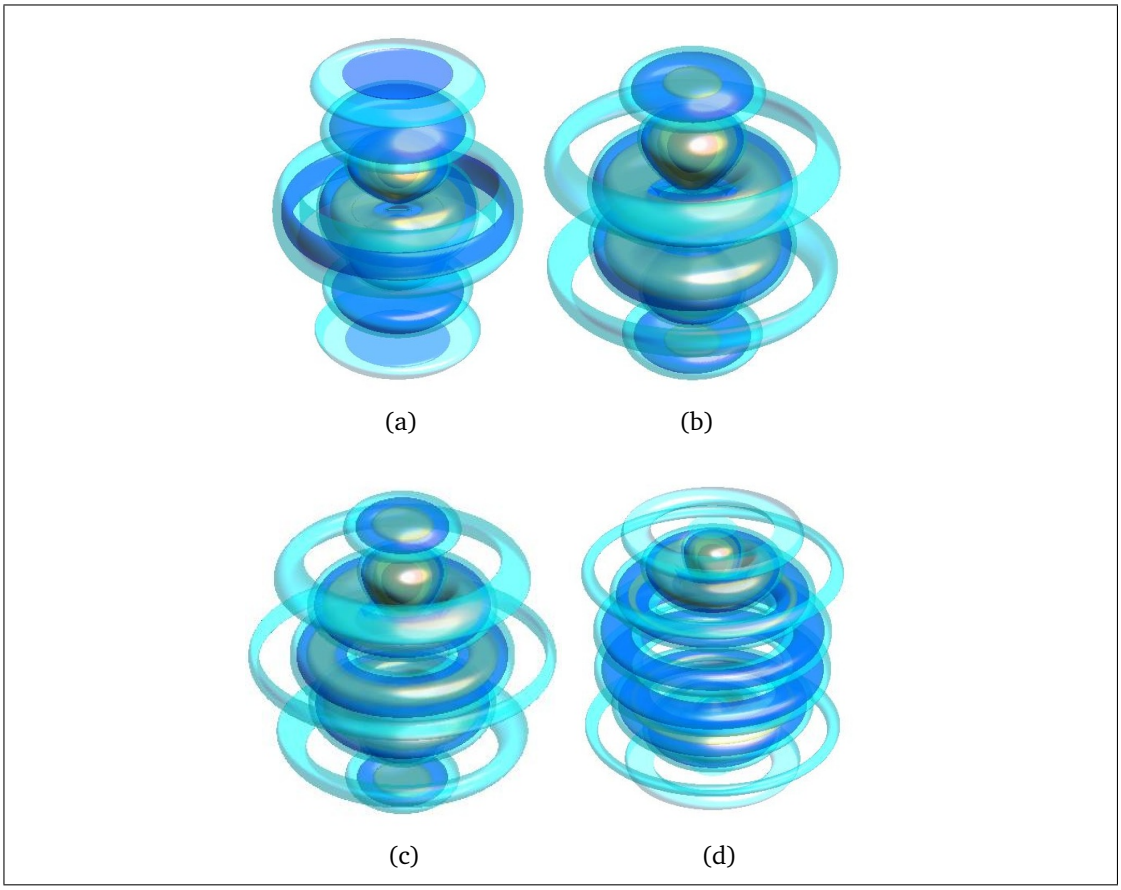

Figure 4.3: Intensity iso-surfaces corresponding to higher order optical bullets having $m = 0$ when: (a) $\ell = 2$, (b) $\ell = 3$, (c) $\ell = 4$, (d) $\ell = 7$

If we assume a state with finite spin ($m \neq 0$), an internal power flow will be present in the wavepacket arising from its exp $[im\phi]$ dependence. Figure 4.4a depicts the iso-intensity plot of an $\ell = m = +2$ bullet while Fig. 4.4b shows its corresponding internal power circulation, $\vec{S_r}$, which happens in this case to be clockwise. As would be anticipated, for $m = -2$ we obtain the same iso-intensity plot while the power circulation is counter-clockwise (Fig. 4.4c).

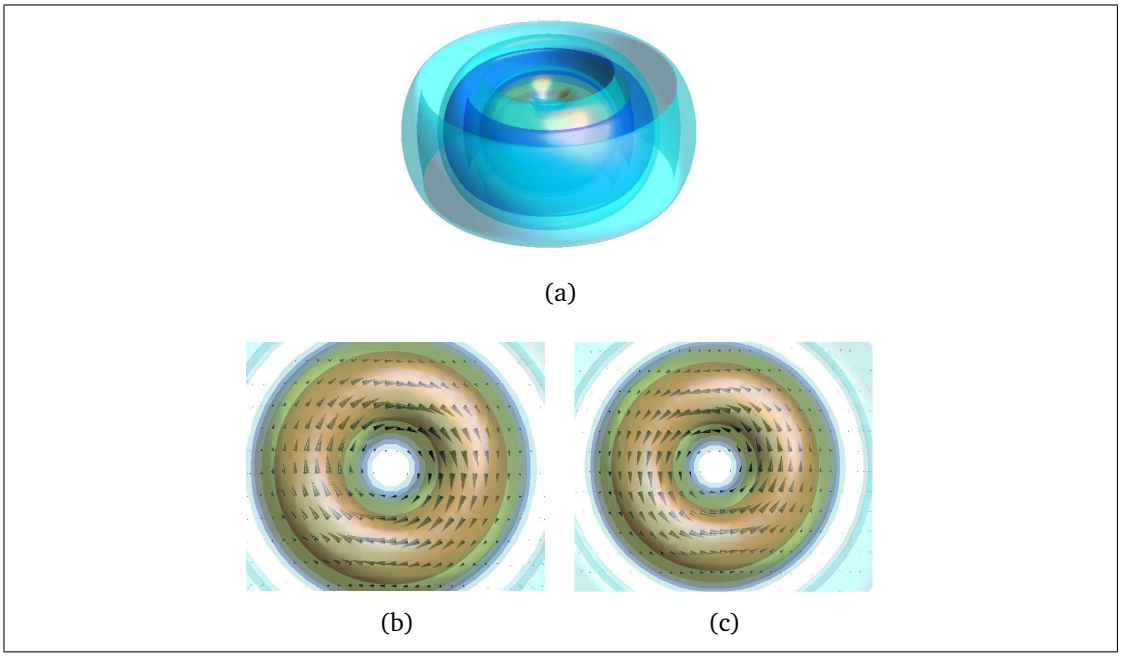

Figure 4.4: (a) Intensity iso-surfaces of an $\ell = 2$; $m = \pm 2$ optical bullet. (b) Top view of power circulation when $m = +2$. (c) Power circulation in this same state when $m = -2$.

This leads to the possibility of realizing superpositions (e.g. $\exp\left[+im\phi\right]$]+$\exp\left[-im\phi\right]$) of spatio-temporal bullets that share the same ℓ number and opposite “spin" numbers, m. If for example $\ell = 2$ and $m = \pm 1$, the wavepacket will have a four-fold symmetry (Fig. 4.5a) and it will be d_{YT} symmetric. On the other hand, a d_{XY} symmetric wavefunction will be similar to the one shown Fig. 4.5b for characteristic indices $\ell = 2$ and $m = \pm 2$.

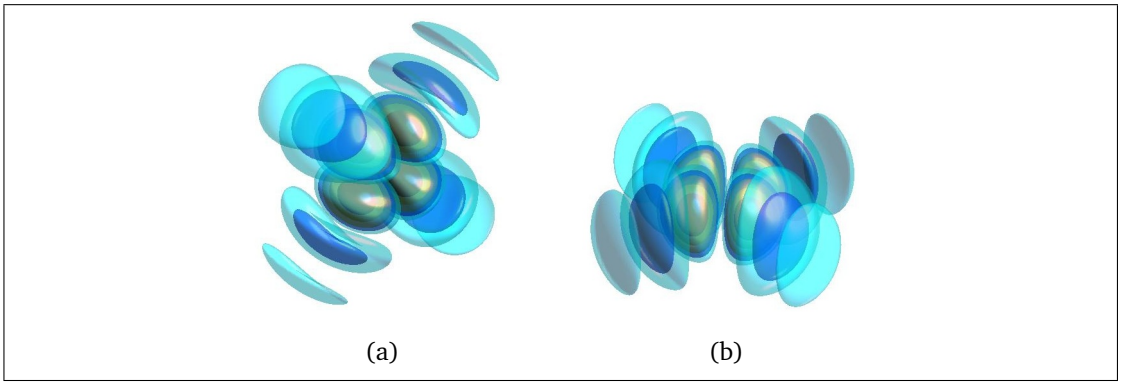

Figure 4.5: Superimposing optical bullets with $\ell = 2$; $m = \pm m_0$. (a) Intensity iso-surfaces with $m_0 = 1$ (b) Isosurfaces with $m_0 = 2$.

In principle, a superposition of two such spatio-temporal hydrogen-like optical bullets that have identical “quantum numbers", ℓ and m, but with slightly different propagation constants ($\alpha_1 \approx \alpha_2$) can lead to a “breathing” wavepacket. If, on the other hand, these two bullets exhibit opposite spins, $\pm m$, then the resulting intensity pattern rotates during propagation with period of $Z_0 = 2\pi/\left|\alpha_2^2 - \alpha_1^2\right|$. This behavior is illustrated in Fig. 4.6 where a spinning optical bullet was generated with two almost degenerate states having $\ell = 2$, $m = \pm 2$ and $\alpha_1 \approx \alpha_2$.

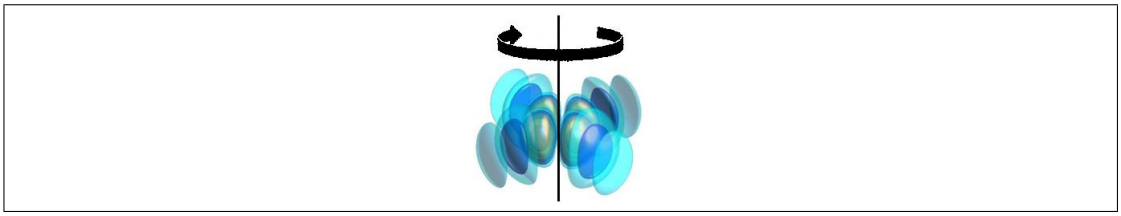

Figure 4.6: A rotating optical light bullet.

4.4 Propagation dynamics of energy apodized light bullets

It is straightforward to show that the optical bullets presented in this paper carry infinite energy. In other words, these spatio-temporal waves happen to be dispersion-diffraction free because they are associated with an infinite norm (very much like plane waves). In practice, any optical bullet can only involve finite energy. As a result, it is important to study the dynamics of this family of optical waves when they are appropriately apodized since it is necessary for their generation. In this case, a truncated bullet is expected to eventually expand in space and time depending on the degree of the apodization itself. Nevertheless, the bigger the space-time aperture is, the longer these bullets will maintain their features and the slower they will deteriorate or expand. In this section, we assume that the apodization is carried out in a Gaussian fashion [24, 62]. To analyze these dynamics we recall that in all cases the electric field envelope obeys equation (4.2). We also note that in $3D$ a Gaussian wavepacket of the form $G(X,Y,T;Z=0) = \exp\left(-R^2/w^2\right)$ satisfies Eq. (4.2) and evolves according to the analytical solution:

$$G(X,Y,T;Z) = \frac{1}{\mu^{3/2}(Z)} \exp\Big(-\frac{X^2+Y^2+T^2}{w^2\mu(Z)}\Big), \tag{4.13}$$

where $\mu(Z) = 1+4iZ/w^2$. Let us now assume that a certain envelope, $\tilde{\psi}(X,Y,T;Z)$, satisfies Eq. (4.2). In that case, it is straightforward to show that its Gaussian apodized counterpart also satisfies Eq.(4.2), that is:

$$\psi(X,Y,T;Z) = \frac{1}{\mu^{3/2}(Z)} \exp\left(\frac{-R^2}{w^2\mu(Z)}\right)\tilde{\psi}(\tilde{X},\tilde{Y},\tilde{T};\tilde{Z}) \tag{4.14}$$

where the new coordinates appearing in Eq. (4.14) have been renormalized with respect to $\mu(Z)$, i.e., $(\tilde{X},\tilde{Y},\tilde{T},\tilde{Z}) = (X,Y,T,Z)/\mu(Z)$. Equation (4.14) is general and holds in all cases. In the specific case of the apodized hydrogen-like optical bullets discussed here, (4.14) leads to:

$$\begin{aligned}\tilde{\psi} = \frac{1}{\mu^{3/2}(Z)} \exp\left(\frac{-R^2}{w^2\mu(Z)}\right) \cdot \psi_0\sqrt{2\pi} j_\ell(\alpha\tilde{R}) P_\ell^m(\cos\tilde{\theta}) \\ \times \exp\left[im\tilde{\phi}\right] \exp\left[-i\alpha^2\tilde{Z}\right]\end{aligned} \tag{4.15}$$

Where the spherical coordinates, $(\tilde{R},\tilde{\theta},\tilde{\phi})$ are associated with the coordinates $(\tilde{X},\tilde{Y},\tilde{T};\tilde{Z})$ and are given by the relations $\tilde{R} = R/\mu(Z)$, $\tilde{\theta} = \theta$, $\tilde{\phi} = \phi$. Figure 4.7 displays a $Y = 0$ intensity cross section at different diffraction lengths for equation (4.15) with $\ell = 2$, $m = 0$, $\alpha = 1$, $\psi_0 = 1$, $w = 2$.

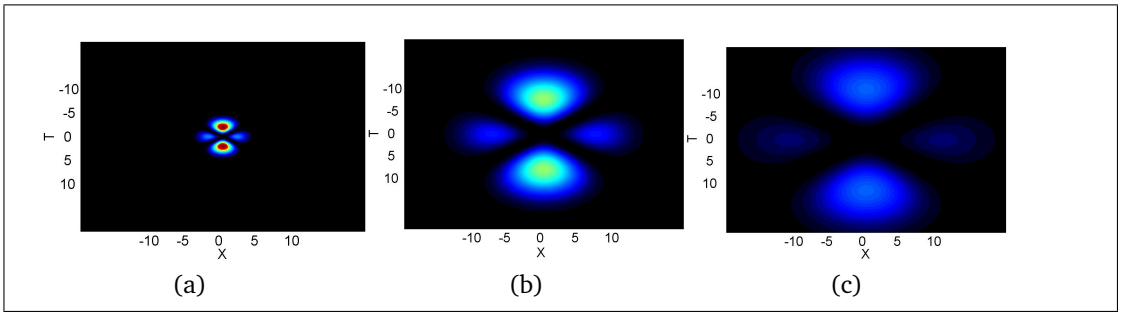

Figure 4.7: Propagation dynamics of an apodized hydrogen-like bullet with $\ell = 2; m = 0$ after a normalized distance of (a) $Z = 0$, (b) $Z = 2.66$, (c) $Z = 4$. Values are normalized to the maximum value of the bullet which occurs at $Z = 0$

As Fig. 4.7 clearly indicates, the apodized optical bullet eventually expands during propagation. This expansion can of course be slowed down by increasing the Gaussian apodization width, w.

4.5 Optical bullets resulting from a spherical superposition on Archimedean and Platonic solids

In general, any non-spreading spatio-temporal wavepacket can be synthesized through a suitable superposition of "plane wave solutions" in the normalized $K_X, K_Y, \bar{\Omega}$ space as long as these points lie on a sphere (where in this last expression $\bar{\Omega} = \Omega\tau_0$). This can be understood from Eq. (4.2), by adopting invariant solutions of the form $\psi = \exp\left(-i\alpha^2 Z\right)\exp\left[i\left(K_X X + K_Y Y - \bar{\Omega}T\right)\right]$. For this case $K_X^2 + K_Y^2 + \bar{\Omega}^2 = \alpha^2$, i.e. the K_X, K_Y, $\bar{\Omega}$ points should indeed lie on a sphere of radius α. Therefore, any superposition of such "plane wave solutions" will also remain also invariant as long as they share the same sphere of radius α in reciprocal space. Following this approach, infinitely many realizations of such invariant optical bullets are attainable. One such possibility is to consider polyhedra that happen to be inscribable on a sphere such as the Platonic or Archimedean solids. In this case, the field envelope of the bullet resulting from this superposition can be obtained by:

$$\psi = \exp\left(-i\alpha^2 Z\right)\sum_j \exp\left(i\vec{Q}_j \cdot \vec{R}\right) \tag{4.16}$$

where $\vec{Q}_j$ represents the reciprocal vertices $\vec{Q} = \left(K_X, K_Y, -\bar{\Omega}\right)$ on this sphere. Figure 4.8a displays the vertices of a Platonic regular hexahedron on a reciprocal space unit sphere occupying the sites $(\pm 1/\sqrt{3}, \pm 1/\sqrt{3}, \pm 1/\sqrt{3})$. Similarly, the vertices corresponding to an octahedron and dodecahedron are depicted in Figs. 4.8b and 4.8c. The respective iso-intensity plots of the spatio-temporal optical bullets that are generated from these three polyhedra are shown in Figs. 4.8d-4.8f.

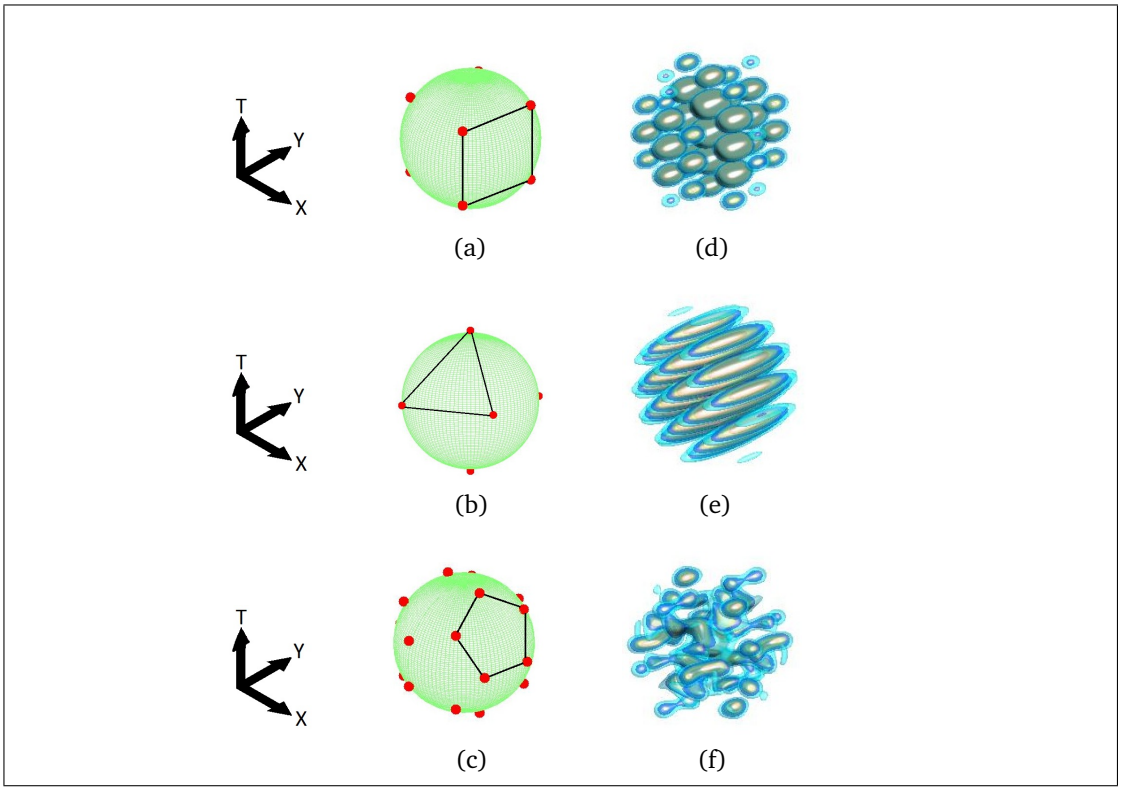

Figure 4.8: The vertices of a (a) regular hexahedron (b) octahedron (c) and dodecahedron inscribed in a Q-sphere. (d-f) The corresponding iso-intensity patterns generated from these arrangements.

4.6 Fourier spectra of apodized spatio-temporal bullets

Fourier spectra provide valuable physical insight not only about the structure of diffraction/dispersion-free bullets, but also dictate the requirements concerning their realization in laboratory experiments. In this section, we provide a general analytical expression for the Fourier spectrum of a Gaussian apodized spatio-temporal bullet that obeys (4.2). More specifically we obtain the spectrum at the origin $Z = 0$, in which case the initial field envelope of such a bullet is given by $\psi(X,Y,T,Z=0) = \psi_B(X,Y,T,Z=0)\exp\left(-R^2/w^2\right)$. In general, a non-spreading spatio-temporal wavepacket can be described as a Fourier superposition of plane waves in spherical coordinates. Note that in a spherical reciprocal space, $K_X = K_R\sin\theta\cos\phi, K_Y = K_R\sin\theta\sin\phi, \bar{\Omega} = -K_R\cos\theta$. In addition, in this same

domain, the spatio-temporal frequencies of a non-spreading wavepacket satisfying (4.2) lie on the surface of a sphere, $K_X^2 + K_Y^2 + \bar{\Omega}^2 = \alpha^2$, hence its spectrum can be described through the general function $\delta(K_R - \alpha)\zeta(\phi, \theta)$. In this case,

$$\psi_B(X, Y, T; Z = 0) = \frac{1}{(2\pi)^3} \int_0^\infty \int_0^\pi \int_0^{2\pi} \mathrm{d}K_R \mathrm{d}\phi \mathrm{d}\theta \left[K_R^2 \sin\theta \delta(K_R - \alpha)\zeta(\phi, \theta) \right] \times \exp\left(iK_R[X\cos\phi\sin\theta + Y\sin\phi\sin\theta + T\cos\theta]\right) \tag{4.17}$$

Thus,

$$\psi_B(X, Y, T; Z = 0) = \frac{1}{(2\pi)^3} \int_0^{2\pi} \mathrm{d}\phi \int_0^\pi \mathrm{d}\theta \left[\zeta(\phi, \theta)\alpha^2 \sin\theta \right] \times \exp\left(i\alpha[X\cos\phi\sin\theta + Y\sin\phi\sin\theta + T\cos\theta]\right) \tag{4.18}$$

Given that this light bullet of (4.18) is apodized in a Gaussian fashion with width, w, its Fourier transform can be obtained from

$$\Psi(K_X, K_Y, \bar{\Omega}) = \int_{-\infty}^\infty \int_{-\infty}^\infty \int_{-\infty}^\infty \mathrm{d}X \mathrm{d}Y \mathrm{d}T \exp\left(-\frac{X^2 + Y^2 + T^2}{w^2} \right) \times \psi_B(X, Y, T; Z = 0) \exp\left[-i\left(K_X X + K_Y Y - \bar{\Omega} T \right) \right] \tag{4.19}$$

Upon substituting (4.18) into (4.19) for $\psi_B(X, Y, T; Z = 0)$, all terms which do not depend on X, Y, or T may be carried out of the Fourier integral. Hence,

$$\Psi(K_X, K_Y, \bar{\Omega}) = \frac{1}{(2\pi)^3} \int_0^{2\pi} \mathrm{d}\phi \int_0^\pi \mathrm{d}\theta \left[\zeta(\phi, \theta)\alpha^2 \sin\theta \right] \times \int_{-\infty}^\infty \int_{-\infty}^\infty \int_{-\infty}^\infty \exp\left(-\frac{X^2 + Y^2 + T^2}{w^2} \right) \times \exp\left(i\alpha[X\cos\phi\sin\theta + Y\sin\phi\sin\theta + T\cos\theta]\right) \times \exp\left[-i\left(K_X X + K_Y Y - \bar{\Omega} T \right) \right] \mathrm{d}X \mathrm{d}Y \mathrm{d}T \tag{4.20}$$

where now in (4.20), K_X, K_Y, and $\bar{\Omega}$ range from $(-\infty, \infty)$. By introducing the auxiliary reciprocal variables, $\Xi_X = K_X - \alpha\sin\theta\cos\phi$, $\Xi_Y = K_Y - \alpha\sin\theta\sin\phi$, and

$\Xi_T = -\bar{\Omega} - \alpha\cos\theta$ equation (4.20) becomes:

$$\begin{aligned}\Psi(K_X,K_Y,\bar{\Omega}) = \frac{1}{(2\pi)^3}\int_0^{2\pi} \mathrm{d}\phi \int_0^{\pi} \mathrm{d}\theta \left[\zeta(\phi,\theta)\alpha^2\sin\theta\right] \\ \times \int_{-\infty}^{\infty}\int_{-\infty}^{\infty}\int_{-\infty}^{\infty} \exp\left(-\frac{X^2+Y^2+T^2}{w^2}\right) \\ \times \exp\left[-i\left(\Xi_X X + \Xi_Y Y + \Xi_T T\right)\right]\mathrm{d}X\,\mathrm{d}Y\,\mathrm{d}T\end{aligned} \tag{4.21}$$

The Fourier integrations in (4.21) can now be performed and lead to:

$$\begin{aligned}\Psi(K_X,K_Y,\bar{\Omega}) = \frac{1}{(2\pi)^3}\int_0^{2\pi} \mathrm{d}\phi \int_0^{\pi} \mathrm{d}\theta \left[\zeta(\phi,\theta)\alpha^2\sin\theta\right] \\ \times w^3\pi^{3/2}\exp\left[-\frac{w^2}{4}\left(\Xi_X^2+\Xi_Y^2+\Xi_T^2\right)\right]\end{aligned} \tag{4.22}$$

Substituting the original expressions for the auxiliary parameters, Ξ_X, Ξ_Y, and Ξ_T, equation (4.22) can be rewritten as follows:

$$\begin{aligned}\Psi(K_X,K_Y,\bar{\Omega}) = \frac{w^3\pi^{3/2}e^{-\left(w^2/4\right)\left(\alpha^2+K_X^2+K_Y^2+\bar{\Omega}^2\right)}}{(2\pi)^3} \\ \times \int_0^{2\pi} \mathrm{d}\phi \int_0^{\pi} \mathrm{d}\theta \left[\zeta(\phi,\theta)\alpha^2\sin\theta\right] \\ \times \exp\left[i\alpha\left(\frac{w^2}{2i}\right)\left(K_X\cos\phi\sin\theta + K_Y\sin\phi\sin\theta - \bar{\Omega}\cos\theta\right)\right]\end{aligned} \tag{4.23}$$

From (4.23) and (4.18), one finally obtains the Fourier spectrum of these apodized bullets which is simply given in terms of their original envelope, ψ_B, where $[X,Y,T] \rightarrow \left(\frac{w^2}{2i}\right)[K_X,K_Y,-\bar{\Omega}]$. Therefore, the end result is:

$$\begin{aligned}\Psi(K_X,K_Y,\bar{\Omega}) = \left(\pi w^2\right)^{3/2} e^{-\left(w^2/4\right)\left(\alpha^2+K_X^2+K_Y^2+\bar{\Omega}^2\right)} \\ \times \psi_B\left(\frac{w^2}{2i}K_X, \frac{w^2}{2i}K_Y, -\frac{w^2}{2i}\bar{\Omega}\right)\end{aligned} \tag{4.24}$$

Equation (4.24) states that if an invariant solution to (4.2) is known, then the

Fourier transform of its Gaussian apodized version is immediately known. We now see that the Fourier transforms of all the hydrogen-like bullets introduced earlier can be readily obtained by combining equations (4.12) and (4.24). As an example, consider the simplest hydrogen-like bullet, for which $\ell = m = 0$, and whose field profile is given by $\psi_0\sqrt{2\pi}j_0(\alpha R) = \psi_0\sqrt{2\pi}\sin(\alpha R)/\alpha R$. Using (4.24) we can immediately obtain the corresponding Gaussian apodized Fourier spectrum:

$$\Psi(K_X, K_Y, \bar{\Omega}) \propto we^{-\left(w^2/4\right)\left(\alpha^2+K_R^2\right)} \times \frac{\sinh\left(w^2\alpha K_R/2\right)}{\alpha K_R} \tag{4.25}$$

where $K_R^2 = K_X^2 + K_Y^2 + \bar{\Omega}^2$. Three reciprocal space isosurfaces for both the $\ell = m = 0$ and $\ell = 1, m = 0$ cases are plotted for different degrees of Gaussian apodization (Fig. 4.9 and Fig. 4.10). As can be seen in Fig. 4.9, in the limit $w \to \infty$, the thickness of the surfaces become infinitesimally small, thus approaching a radius of α. As expected, in this limit the light bullet in Fig. 4.9 converges to the spectrum of the O-wave displayed in Fig. 4.1. This behavior can be readily understood from Eq. (4.25). Meanwhile the spectrum of a p_T-like orbital that involves two lobes is displayed in Fig. 4.10.

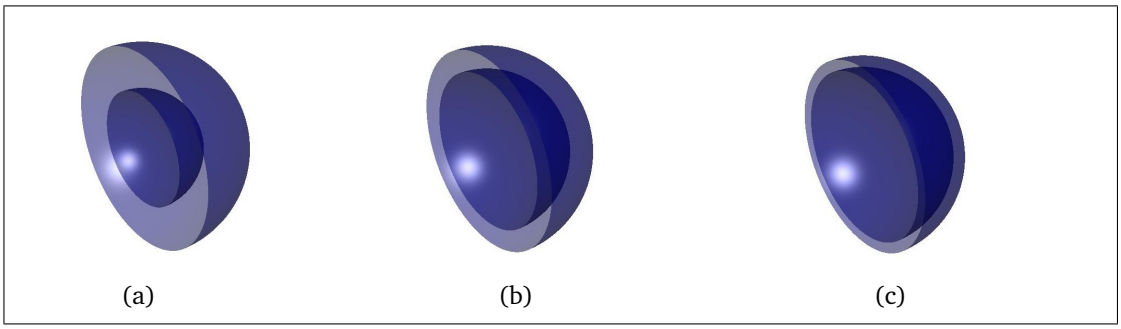

Figure 4.9: Isosurface spectrum plots of the $\ell = m = 0$ hydrogen bullet with various degrees of Gaussian apodization. The spherical spectrum has been sectioned in half so that the shell thickness can be viewed a) $w = 5$. b) $w = 10$. c) $w = 20$. In the limit that $w \to \infty$ the shell thickness becomes infinitesimally small representing the spectrum of the O-wave.

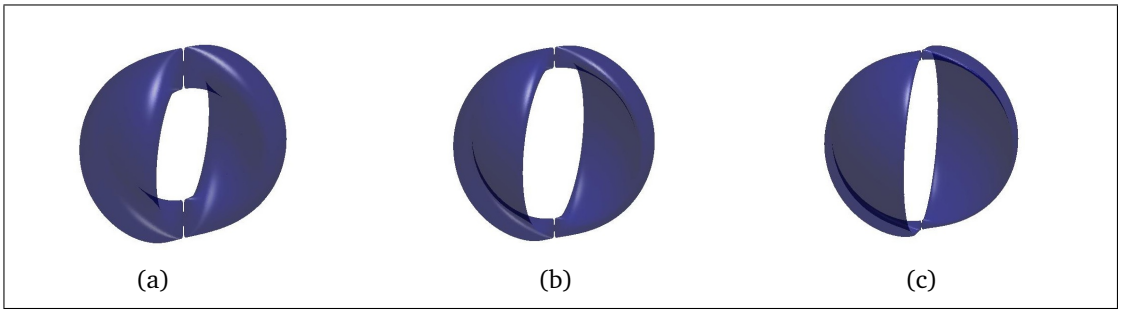

Figure 4.10: Isosurface spectrum plots of the $\ell = 1, m = 0$ hydrogen bullet with various degrees of Gaussian apodization. The spherical spectrum has been sectioned in half so that the shell thickness can be viewed a) $w = 5$. b) $w = 10$. c) $w = 20$.

References

[1] J. Durnin, J. J. Miceli, and J. H. Eberly, "Diffraction-free beams," *Phys. Rev. Lett.*, vol. 58, pp. 1499–1501, Apr 1987. 1, 7, 14

[2] G. A. Siviloglou and D. N. Christodoulides, "Accelerating finite energy airy beams," *Opt. Lett.*, vol. 32, pp. 979–981, Apr 2007. 1, 16, 17, 25

[3] R. M. Herman and T. A. Wiggins, "Production and uses of diffractionless beams," *J. Opt. Soc. Am. A*, vol. 8, pp. 932–942, Jun 1991. 1, 14

[4] M. Erdelyi, Z. L. Horvath, G. Szabo, Z. Bor, F. K. Tittel, J. R. Cavallaro, and M. C. Smayling, "Generation of diffraction-free beams for applications in optical microlithography," *Journal of Vacuum Science Technology B: Microelectronics and Nanometer Structures*, vol. 15, pp. 287 –292, mar 1997. 1

[5] J. yu Lu and J. F. Greenleaf, "Diffraction-limited beams and their applications for ultrasonic imaging and tissue characterization (invited paper)," vol. 1733, pp. 92–119, SPIE, 1992. 1

[6] D. Christodoulides, "Diffraction." University Lecture, 2011. 1, 3

[7] D. McGloin and K. Dholakia, "Bessel beams: Diffraction in a new light," *Contemporary Physics*, vol. 46, no. 1, pp. 15–28, 2005. 2, 9, 14, 15

[8] D. M. G. Moharam, "Em field theory and maxwell's equations." University Lecture, 2010. 2

[9] I. Kaminer, R. Bekenstein, and M. Segev, "Non-paraxial accelerating beams," in *CLEO: QELS-Fundamental Science*, p. QM3E.3, Optical Society of America, 2012. 4

[10] D. M. G. Moharam, “Propagation of gaussian beams.” University Lecture, 2010. 4, 5

[11] J. Durnin, “Exact solutions for nondiffracting beams. i. the scalar theory,” *J. Opt. Soc. Am. A*, vol. 4, pp. 651–654, Apr 1987. 6, 7

[12] E. Whittaker, “On the partial differential equations of mathematical physics,” *Mathematische annalen*, vol. 57, no. 3, pp. 333–355, 1903. 6

[13] F. W. Olver, D. W. Lozier, R. F. Boisvert, and C. W. Clark, *NIST Handbook of Mathematical Functions*. New York, NY, USA: Cambridge University Press, 1st ed., 2010. 6

[14] D. DeBeer, S. R. Hartmann, and R. Friedberg, “Comment on "diffraction-free beams",” *Phys. Rev. Lett.*, vol. 59, pp. 2611–2611, Nov 1987. 8

[15] J. E. Harvey and J. L. Forgham, “The spot of arago: New relevance for an old phenomenon,” *American Journal of Physics*, vol. 52, no. 3, pp. 243–247, 1984. 8

[16] P. Sprangle and B. Hafizi, “Comment on nondiffracting beams,” *Phys. Rev. Lett.*, vol. 66, pp. 837–837, Feb 1991. 8

[17] J. Durnin, J. J. Miceli, and J. H. Eberly, “Durnin, miceli, and eberly reply,” *Phys. Rev. Lett.*, vol. 59, pp. 2612–2612, Nov 1987. 8

[18] J. Durnin, J. J. Miceli, and J. H. Eberly, “Durnin, miceli, and eberly reply,” *Phys. Rev. Lett.*, vol. 66, pp. 838–838, Feb 1991. 8

[19] J. Durnin, J. J. M. Jr., and J. H. Eberly, “Comparison of bessel and gaussian beams,” *Opt. Lett.*, vol. 13, pp. 79–80, Feb 1988. 8, 14

[20] Y. Lin, W. Seka, J. H. Eberly, H. Huang, and D. L. Brown, “Experimental investigation of bessel beam characteristics,” *Appl. Opt.*, vol. 31, pp. 2708–2713, May 1992. 10

[21] Z. Bouchal, J. Wagner, and M. Chlup, “Self-reconstruction of a distorted non-diffracting beam,” *Optics Communications*, vol. 151, no. 4âĂŞ6, pp. 207 – 211, 1998. 12

[22] M. Born and E. Wolf, *Principles of Optics*. Pergamon Press, New York, 1980. 12

[23] D. Christodoulides, "Diffraction-free beams and waves." MURI school lecture, 2011. 13

[24] F. Gori, G. Guattari, and C. Padovani, "Bessel-gauss beams," *Optics Communications*, vol. 64, no. 6, pp. 491 – 495, 1987. 13, 34

[25] J. H. MCLEOD, "The axicon: A new type of optical element," *J. Opt. Soc. Am.*, vol. 44, pp. 592–592, Aug 1954. 14

[26] G. Scott and N. McArdle, "Efficient generation of nearly diffraction-free beams using an axicon," *SPIE Optical Engineering*, vol. 31, pp. 2640–2643, Dec 1992. 14

[27] S. Monk, J. Arlt, D. Robertson, J. Courtial, and M. Padgett, "The generation of bessel beams at millimetre-wave frequencies by use of an axicon," *Optics Communications*, vol. 170, no. 4âĂŞ6, pp. 213 – 215, 1999. 15

[28] A. J. Cox and D. C. Dibble, "Nondiffracting beam from a spatially filtered fabry-perot resonator," *J. Opt. Soc. Am. A*, vol. 9, pp. 282–286, Feb 1992. 15

[29] J. Turunen, A. Vasara, and A. T. Friberg, "Holographic generation of diffraction-free beams," *Appl. Opt.*, vol. 27, pp. 3959–3962, Oct 1988. 15

[30] M. V. Berry and N. L. Balazs, "Nonspreading wave packets," *American Journal of Physics*, vol. 47, no. 3, pp. 264–267, 1979. 16, 17

[31] J. Broky, G. A. Siviloglou, A. Dogariu, and D. N. Christodoulides, "Self-healing properties of optical airy beams," *Opt. Express*, vol. 16, pp. 12880–12891, Aug 2008. 17

[32] G. A. Siviloglou, J. Broky, A. Dogariu, and D. N. Christodoulides, "Ballistic dynamics of airy beams," *Opt. Lett.*, vol. 33, pp. 207–209, Feb 2008. 17, 20, 21

[33] I. M. Besieris, A. M. Shaarawi, and R. W. Ziolkowski, "Nondispersive accelerating wave packets," *American Journal of Physics*, vol. 62, no. 6, pp. 519–521, 1994. 17

[34] G. A. Siviloglou, J. Broky, A. Dogariu, and D. N. Christodoulides, "Observation of accelerating airy beams," *Phys. Rev. Lett.*, vol. 99, p. 213901, Nov 2007. 20

[35] D. M. Greenberger, "Comment on "nonspreading wave packets"," *American Journal of Physics*, vol. 48, no. 3, pp. 256–256, 1980. 20

[36] D. M. Greenberger and A. W. Overhauser, "Coherence effects in neutron diffraction and gravity experiments," *Rev. Mod. Phys.*, vol. 51, pp. 43–78, Jan 1979. 20

[37] L. I. Schiff, *Quantum mechanics / Leonard I. Schiff*. McGraw-Hill, New York :, 3rd ed. ed., 1968. 20

[38] P. Polynkin, M. Kolesik, J. V. Moloney, G. A. Siviloglou, and D. N. Christodoulides, "Curved plasma channel generation using ultraintense airy beams," *Science*, vol. 324, no. 5924, pp. 229–232, 2009. 21

[39] Q. Luo, H. Xu, S. Hosseini, J.-F. Daigle, F. ThÃľberge, M. Sharifi, and S. Chin, "Remote sensing of pollutants using femtosecond laser pulse fluorescence spectroscopy," *Applied Physics B: Lasers and Optics*, vol. 82, pp. 105–109, 2006. 10.1007/s00340-005-2008-x. 21

[40] H. Xu, J. Daigle, Q. Luo, and S. Chin, "Femtosecond laser-induced nonlinear spectroscopy for remote sensing of methane," *Applied Physics B: Lasers and Optics*, vol. 82, pp. 655–658, 2006. 10.1007/s00340-005-2123-8. 21

[41] C. D'Amico, A. Houard, M. Franco, B. Prade, A. Mysyrowicz, A. Couairon, and V. T. Tikhonchuk, "Conical forward thz emission from femtosecond-laser-beam filamentation in air," *Phys. Rev. Lett.*, vol. 98, p. 235002, Jun 2007. 21

[42] C. Hauri, W. Kornelis, F. Helbing, A. Heinrich, A. Couairon, A. Mysyrowicz, J. Biegert, and U. Keller, "Generation of intense, carrier-envelope phase-locked few-cycle laser pulses through filamentation," *Applied Physics B: Lasers and Optics*, vol. 79, pp. 673–677, 2004. 10.1007/s00340-004-1650-z. 21

[43] T. Juhasz, F. Loesel, R. Kurtz, C. Horvath, J. Bille, and G. Mourou, "Corneal refractive surgery with femtosecond lasers," *Selected Topics in Quantum Electronics, IEEE Journal of*, vol. 5, pp. 902 –910, jul/aug 1999. 21

[44] M. Mlejnek, E. M. Wright, and J. V. Moloney, "Dynamic spatial replenishment of femtosecond pulses propagating in air," *Opt. Lett.*, vol. 23, pp. 382–384, Mar 1998. 21

[45] N. K. Efremidis and D. N. Christodoulides, "Abruptly autofocusing waves," *Opt. Lett.*, vol. 35, pp. 4045–4047, Dec 2010. 21

[46] K. Makris, "Beam propagation methods." Ph.D notes, 2006. 23

[47] P. Zhang, J. Prakash, Z. Zhang, M. S. Mills, N. K. Efremidis, D. N. Christodoulides, and Z. Chen, "Trapping and guiding microparticles with morphing autofocusing airy beams," *Opt. Lett.*, vol. 36, pp. 2883–2885, Aug 2011. 23

[48] I. Chremmos, N. K. Efremidis, and D. N. Christodoulides, "Pre-engineered abruptly autofocusing beams," *Opt. Lett.*, vol. 36, pp. 1890–1892, May 2011. 23

[49] B. A. Malomed, D. Mihalache, F. Wise, and L. Torner, "Spatiotemporal optical solitons," *Journal of Optics B: Quantum and Semiclassical Optics*, vol. 7, no. 5, p. R53, 2005. 25

[50] Y. Silberberg, "Collapse of optical pulses," *Opt. Lett.*, vol. 15, pp. 1282–1284, Nov 1990. 25

[51] S. Longhi, "Localized subluminal envelope pulses in dispersive media," *Opt. Lett.*, vol. 29, pp. 147–149, Jan 2004. 25, 31

[52] J.-Y. Lu and J. F. Greenleaf, "Nondiffracting x-waves: exact solutions to free-space scalar wave equation and their finite aperture realizations," *IEEE Trans. Ultrason. Ferroelectr. Freq. Control*, vol. 39, pp. 19–31, 1992. 25

[53] P. Di Trapani, G. Valiulis, A. Piskarskas, O. Jedrkiewicz, J. Trull, C. Conti, and S. Trillo, "Spontaneously generated x-shaped light bullets," *Phys. Rev. Lett.*, vol. 91, p. 093904, Aug 2003. 25

[54] D. N. Christodoulides, N. K. Efremidis, P. D. Trapani, and B. A. Malomed, "Bessel x waves in two- and three-dimensional bidispersive optical systems," *Opt. Lett.*, vol. 29, pp. 1446–1448, Jul 2004. 25

[55] M. A. Porras and P. Di Trapani, "Localized and stationary light wave modes in dispersive media," *Phys. Rev. E*, vol. 69, p. 066606, Jun 2004. 25, 31

[56] M. R. H. Sonajalg and P. Saari, "Demonstration of the bessel-x pulse propagating with strong lateral and longitudinal localization in a dispersive medium," *Opt. Lett.*, vol. 22, pp. 310–312, Mar 1997. 25

[57] D. N. C. A. Chong, W. H. Renninger and F. W. Wise, "Airy-bessel wave packets as versatile linear light bullets," *Nature Photonics*, vol. 4, p. 103, 2010. 25

[58] X. Liu, L. J. Qian, and F. W. Wise, "Generation of optical spatiotemporal solitons," *Phys. Rev. Lett.*, vol. 82, pp. 4631–4634, Jun 1999. 26

[59] M. Dallaire, N. McCarthy, and M. Piché, "Spatiotemporal bessel beams:theory and experiments," *Opt. Express*, vol. 17, pp. 18148–18164, Sep 2009. 26

[60] S. López-Aguayo, Y. V. Kartashov, V. A. Vysloukh, and L. Torner, "Method to generate complex quasinondiffracting optical lattices," *Phys. Rev. Lett.*, vol. 105, p. 013902, Jun 2010. 26

[61] O. V. Borovkova, Y. V. Kartashov, V. E. Lobanov, V. A. Vysloukh, and L. Torner, "General quasi-nonspreading linear three-dimensional wave packets," *Opt. Lett.*, vol. 36, pp. 2176–2178, Jun 2011. 26

[62] M. D. I.-C. J. C. Gutirrez-Vega and S. Chavez-Cerda, "Alternative formulation for invariant optical fields: Mathieu beams," *Opt. Lett.*, vol. 25, pp. 1493–1495, Oct 2000. 34